NASA Contractor Report No. 66676

MATHEMATICAL MODEL PREDICTIONS AND OPTIMIZATION STUDY OF THE GAMMA-RAY ATMOSPHERIC DENSITY SENSOR

D. R. Whitaker and R. P. Gardner

Prepared for

Langley Research Center
National Aeronautics and Space Administration

(Prepared under Contract No. NAS1-7046, RTI Project No. NU-321, by the Engineering and Environmental Sciences Division of the Research Triangle Institute, Research Triangle Park, North Carolina.)

August 1968

ABSTRACT

Title: Mathematical Model Predictions and Optimization Study of the Gamma-Ray Atmospheric Density Sensor

Authors: D. R. Whitaker and R. P. Gardner

Mathematical models were previously derived to study the response of a gamma-ray backscatter sensor for atmospheric density measurements. These models, developed for a cylindrically symmetrical geometry have been adapted to three-dimensional models having more general application. The models were then integrated with a multivariable search routine to optimize a sensor design for specific missions. Optimum design parameters for a Mars atmosphere density measurement were calculated.

TABLE OF CONTENTS

CONTENTS (Continued)

1. INTRODUCTION

The gamma-ray scattering technique for measuring the atmospheric density surrounding space vehicles has been studied and developed in several experimental and theoretical programs [1,2,3,4] funded by NASA over the past few years. Results of these studies indicate that this technique is feasible and has many advantages. Among these advantages are: (1) fast response time, (2) all gauge components can be installed completely within the space vehicle, (3) large effective sample volume, (4) linear response for densities equal to or less than that at sea level on Earth, and (5) the response is negligibly affected by atmospheric composition or shock waves when the gauge is properly designed.

The primary problem associated with this technique was a high noise level that limited the low-density measurement range of this technique. The source of this noise has been identified [4] as the multiple streaming of gamma-rays and some beta-particle-produced bremsstrahlung from the radioisotope source down the space vehicle walls. Mathematical modeling and experimental studies of this phenomenon have been successfully employed to the extent that the effect of the important parameters governing this source of noise can be assessed. Appropriate gauge and radioisotope source designs that will minimize this noise level for any given set of design restraints imposed by a particular atmospheric density measurement can now be made with the aid of the mathematical models.

In previous work under Contract No. NAS1-5467, theoretical, mathematical models were derived to predict the performance, identify problem areas, and explain the data taken on two flight tests of a gamma-ray scatter gauge. These models were cylindrically symmetrical with a source, conical shield, and a cylindrical scintillation detector mounted on the major axis inside a cone-shaped rocket. Predictions from these models were that the gauge response was linear with atmospheric density, independent of atmospheric composition if

gamma-ray energies larger than 0.1 Mev are employed, affected by atmospheric density as far as 10 meters from the rocket, and independent of shock wave perturbations that are likely to be encountered.

In the present Contract No. NAS1-7046 the work was divided into two phases with the decision to proceed with Phase II contingent on the results of Phase I. Phase I was an experimental verification of the symmetrical models described in an earlier report [3] and an optimum source study. Results of this work verified the models quite well [4] and therefore the decision to proceed with Phase II of this contract was made.

This report presents the results of Phase II of Contract No. NAS1-7046. This work was divided into three tasks. Since an atmospheric density measurement of interest to NASA is that on Mars, the symmetrical models had to be adapted to the non-symmetrical geometry of a Mars atmosphere sensor. This represented the first task of this effort. The second task consisted of designing and testing a master computer program for carrying out a multivariable search of design parameters. Task 3 consisted of running the completed program to obtain optimum design parameters for a Mars atmosphere gauge.

An additional task was added during the Phase II work because the Phase I effort had indicated that the buildup factor necessary for correcting the two-dimensional model predictions of wall streaming was too complex to determine generally by simple correlations with the limited amount of data taken in Phase I. This task consisted of investigating the use of the Monte Carlo technique to determine the multiple scattering of gamma rays down the vehicle walls.

2. DISCUSSION OF APPROACH

The Phase II work was divided into several tasks as discussed in the Introduction. These tasks are quite interrelated since the final objective of the present program is to use computer programs to optimize a Mars atmosphere gauge.

2.1 Conceptual Design Optimization with Mathematical Models

Historically, optimizations with mathematical models have been used extensively in the field of economics, military tactics, and other traditional operations research topics. Recently, applications of these techniques have been made to the optimization of industrial processes. The application of these techniques to the design of measurement devices such as the present application to gamma-ray scatter gauges for atmospheric density measurement is new.

Generally, optimizations with mathematical models involve describing the phenomenon of interest with a mathematical model or models. These models should be capable of predicting the effect of changes in the parameters that are pertinent to the phenomenon. A single desired criterion is established that must be maximized (or minimized) to obtain optimum performance. Various combinations of the pertinent adjustable parameters are used in the mathematical model or models and the optimum criterion is calculated. The particular set of values of the adjustable parameters that maximize (or minimize) the optimum criterion represent the optimum design for the phenomenon being investigated. Various formalized procedures are utilized to establish the "search" pattern that will insure that a true maximum (or minimum) is found with the most efficient computational effort.

It is helpful at this point to examine this optimization procedure in terms of the separable parts and how they are interrelated. Figure 2-1 is a schematic diagram of the optimization procedure. There are six separable parts of the optimization procedure. The "search routine" is the heart of the procedure and is shown in the center. According to the problem "constraints" which are fed

into the search rountine (step 1), values of the "adjustable parameters" are selected (step 2) and inserted into the "mathematical model" (step 3). The mathematical model calculates a "value of the criterion" (step 4) and this value is returned to the search routine (step 5). This entire process is repeated until the search routine decides that a maximum (or minimum) value of the criterion has been reached. At this point the search routine lists the "optimum values of parameters" (step 6). The specific problems associated with the application of this general procedure to the optimum conceptual design of a gamma-ray scatter gauge for measuring the atmospheric density of Mars from a Voyager Probe/Lander is discussed in the following subsections of Sec. 2.

2.2 Application to Gamma-ray Scatter Atmospheric Density Gauges

A discussion of the mathematical model optimization procedure as shown in Fig. 2-1 is given in this subsection to elucidate the more specific problem of applying this technique to the optimum conceptual design of gamma-ray atmospheric density gauges. The "optimum values of the parameters" part is self explanatory and requires no discussion. The obvious criterion for this particular case is the minimum noise-to-signal ratio of the gauge response. The search routine chosen is the Rosenbrock [5] method which is described in more detail in Sec. 4.

The mathematical models used here were modified from the earlier symmetrical models because the proposed Mars atmosphere gauge will not have symmetry about the line connecting the center of the source and center of the detector. This modification of the models to the three-dimensional case represented a significant effort in the present program and will make the models more generally applicable to future problems.

Figure 2-2 schematically shows the major components of a gamma-ray scatter gauge for the measurement of atmospheric density. These include: (1) a source of electromagnetic radiation, (2) a direct transmission shield, (3) a

detector, (4) the electronic components necessary to process the detector response, and (5) the walls of the container that houses all the gauge components. The last two of these components, electronics and container walls, are essentially fixed by the gauge and space vehicle design and are not usually adjustable. The adjustable parameters are primarily concerned with the first three items; the source, the shield, and the detector.

The source of electromagnetic radiation can be either a radioisotope or a machine source. If a radioisotope source is chosen (as in the studies to date), it must be selected on the basis of energy emitted, half-life, specific activity, and availability.

The design of the direct transmission shield depends directly on the radiation source and detector that are chosen. Usually one desires to minimize the total weight of the shield while still eliminating most of the radiation that penetrates the shield and goes directly to the detector. Besides weight considerations, one would also like to optimize the shape and position of the shield for most efficiency.

The detector should be chosen for optimum efficiency. The size and shape of the detector for the present case would be determined on the basis of the optimum signal-to-noise ratio. This depends to a large extent on what source energy and shield design are used. Since the gauge response is almost a direct function of the detector face area, this would indicate that a large detector is desirable. However, the noise due to source direct transmission and cosmic radiation also increases with detector size, indicating a conflicting desirability for a small detector. This is a specific, qualitative example of why one expects to find an optimum design for the gauge. The type of detector (viz. organic crystal, inorganic crystal, proportional gas, etc.) depends upon the overall efficiency for the source gamma-ray energy chosen, the required

ruggedness, dependability, and insensitivity to the probable changes in ambient temperature and pressure.

Besides these design considerations connected directly to the basic components of the gauge, one must also consider such things as: source-detector distance, collimation of source and detector, and discriminator settings. It is obvious from the large number of adjustable parameters and their complicated and highly interrelated effect upon the signal and noise that a search routine used with mathematical models would be a useful method of determining the optimum conceptual design of a gauge.

Constraints are imposed by the specific measurement required. The planned entry speed establishes the necessary gauge response speed or time constant. The expected atmospheric density in conjunction with the gauge time constant determines the source intensity. The time required to reach the destination in conjunction with the maximum allowable initial source intensity determines the lower limit on the source half-life.

The mathematical models required should be capable of relating the predicted signal and noise of a gauge for any combination of the pertinent adjustable parameters. The models should be as accurate as possible consistent with reasonable computation times on a high speed computer.

2.3 Mathematical Model Requirements

To optimize the signal-to-noise ratio one must have models for the signal and all sources of noise in terms of the adjustable parameters previously discussed. By definition, there is only one source of signal, but there are several possible sources of noise. These include: (1) multiple scattering down the space vehicle walls, (2) cosmic radiation, (3) source radiation transmitted through the shield, (4) natural radioactivity in the space vehicle and on Mars, and (5) electronic noise. The last two sources of noise are omitted here as they are probably negligible in relation to the others for the present case. They

could easily be included for other proposed measurement optimizations. Mathematical models for the signal and each of the three sources of noise are derived and discussed in Sec. 3.

In addition to optimizing the signal-to-noise ratio, it was desirable to check the accuracy of the mathematical models by comparing them with the two-dimensional models. Signal response as a function of atmospheric density, source energy, and shock wave pertubations for the three-dimensional model were of interest. Also, detector response as a function of distance from the source and a plot of the number of gamma rays scattered and eventually detected at any distance from the source and detector were desired. Wall streaming response as a function of gamma-ray energy was also of interest.

Comparison of these results with the two-dimensional results would indicate which parameters should be optimized for the final gauge design.

2.4 Application to Gauge for Martian Atmospheric Density Measurement

The specific constraints imposed by the proposed measurement of the Martian atmospheric density can be inferred from a preliminary study made by Giannini Controls Corporation [6]. First of all the proposed Mars gauge is not symmetrical, as already discussed. The other pertinent constraints are only briefly discussed here and no effort is made to thoroughly substantiate them. For a more detailed discussion of these constraints refer to Ref. 6.

Spacecraft weight restrictions and state-of-the-art development of machine sources of electromagnetic radiation indicate that the use of a radioisotope source is desirable for this application. The expected atmospheric density of the Martian atmosphere and the design vehicle entry speed combine to require a source intensity (delivered to Mars) of 20 curies, assuming one gamma ray is emitted per source disintegration. On the basis of efficiency and ability to withstand the expected ambient conditions, the type of detector chosen is a scintillation crystal with photomultiplier. The detector shape is to be a right-circular

cylinder so that state-of-the-art photomultiplier tubes can be efficiently matched to the detector. A schematic drawing of the gauge with pertinent nomenclature is given in Fig. 2-2. The important points to note are that the source and detector are the same distance from the vehicle wall and the wall is considered to be flat with no curvature. These assumptions were made to simplify the mathematical models. They do not seriously affect the generality of the program. Shields are shown at both the source and detector. Collimation of source and detector is not shown since it could be accomplished by many different configurations.

Derivations and discussions of the three-dimensional mathematical models are given in the next section.

3. THREE-DIMENSIONAL MATHEMATICAL MODELS

Mathematical models of the signal and the three sources of noise are derived and discussed separately in this section. In addition, a model for calculating the solid angle subtended by the circular face of a detector from a point at any position and a model for calculating the detector efficiency for any gamma-ray energy and right-circular cylindrical detector are derived and discussed, since these last models were required for use with each of the three-dimensional models for signal and noise.

3.1 Derivation and Discussion of Models

3.1.1 Signal Response Model

A schematic diagram with pertinent nomenclature for the derivation of the signal response model is given in Fig. 3-1. A somewhat unusual coordinate system is used to coincide with the desired collimation limits. This coordinate system uses two of the conventional spherical coordinates, r and Φ, but replaces the usual θ by ψ, which is the angle between the z Cartesian coordinate axis and the r line superimposed on the y-z plane. The origin is taken as the center of the source. Cartesian coordinates are often used in the derivations as well as the r,Φ,ψ coordinates. All three coordinate systems are shown in Fig. 3-1. The relationships between the various coordinate systems are given in Table 3-1.

Figure 3-2 shows the desired integration limits on the coordinate system used in this study. The limits of Φ which are in the x-y plane are Φ_{min} and Φ_{max}. The limits on ψ in the y-z plane are assumed to be symmetrical and equal to ψ_c. The maximum limit on r is taken as r_{max}. The minimum limit on r, $r_{min}(\Phi, \psi)$, depends on the values of ψ and Φ and is taken as the intersection of the Φ,ψ line with the outer face of the space vehicle wall.

The signal response model is derived by identifying separable parts of each gamma-ray path that originates from the source and is scattered by the surrounding atmosphere into the detector. All possible paths are obtained by integrating on r, Φ, and ψ according to the limits just established and shown in Fig. 3-2. This model assumes that only gamma rays scattered once are detected. This has been shown to be a good assumption in the past [3,4] and would be expected to be an even better assumption for the present case since the atmosphere of interest is even less dense than that previously considered. This means that multiple scattering is even less likely.

The first probability, P_1, is the probability that any gamma-ray emitted from the source will be emitted within the differential angles $d\Phi$ and $d\psi$ about the mean angles Φ and ψ and will reach the distance r without being attenuated. From this description P_1 is seen to be:

$$P_1 = \frac{d\psi}{2\pi} \frac{\sin \Phi \, d\Phi}{2} \exp \left[-\mu_t [r - r_{min}(\Phi,\psi)] - \mu_w t'_w (\Phi,\psi)\right] \qquad (3.1.1\text{-}1)$$

where μ_t is the total attenuation coefficient of the atmosphere, in cm^{-1},

$t'_w (\Phi,\psi)$ is the wall thickness through which the gamma-ray must pass when it is traveling in the direction Φ and ψ, in cm,

r is the distance from the source, in cm,

and μ_w is the attenuation coefficient of the wall, in cm^{-1}.

In the studies reported here the μ_w term has been assumed to be one-half of the true value since it is comprised almost entirely of the Compton scattering probability. This assumes that even if a large number of gamma-rays are scattered by the wall, only that half of them that are scattered at angles of $\pi/2$ or larger are lost as potential signal producers. (The low-energy gamma rays of concern in this study scatter essentially symmetrically about the $\pi/2$ plane so that half

of the scatters are at angles greater than $\pi/2$ and subsequently are lost.) The μ_t term is taken as the sum of the Compton scattering and photoelectric probabilities for all the components of the atmosphere. The probability for pair production is not considered since this probability is negligible for gamma-ray energies less than about 2 Mev. This atmospheric attenuation coefficient is given by

$$\mu_t = N_A \rho \sigma_e \sum_{i=1}^{n} w_i Z_i / A_i + N_A \rho \sum_{i=1}^{n} \tau_{ai} w_i / A_i \quad \text{cm}^{-1} \qquad (3.1.1\text{-}2)$$

where N_A is Avogadro's Number, 6.025×10^{23} atoms/g-atom,

ρ is the atmospheric density, in g/cm^3,

σ_e is the total Compton scattering probability per electron, in cm^2/electron,

w_i is the weight fraction of element i,

Z_i is the atomic number of element i,

A_i is the mass number of element i,

τ_{ai} is the photoelectric probability per atom of element i, in cm^2/atom,

and n is the number of elements present in the atmosphere.

The μ_w term is identical to μ_t except that the elements within the space vehicle wall are summed.

The total Compton scattering probability per electron is given by Evans[8] as:

$$\sigma_e = 2\pi r_o^2 \left\{ \frac{1+\alpha}{\alpha^2} \left[\frac{2(1+\alpha)}{1+2\alpha} - \frac{1}{\alpha} \ln(1+2\alpha) \right] + \frac{1}{2\alpha} \ln(1+2\alpha) - \frac{1+3\alpha}{(1+2\alpha)^2} \right\} \text{cm}^2/\text{electron} \qquad (3.1.1\text{-}3)$$

where r_o is the classical electron radius, 2.818×10^{-13} cm,

and α is the gamma-ray energy in Mev divided by the rest-mass energy of an electron (0.511 Mev).

The second probability, P_2, is taken as those gamma rays already described by P_1 that are scattered within the differential distance dr at mean distance r to within the solid angle subtended by the detector.

$$P_2 = [\int_o^{\theta_2} (d\sigma_e/d\theta)\, d\theta - \int_o^{\theta_1} (d\sigma_e/d\theta) d\theta]\, \rho_e\, dr\, F \qquad (3.1.1\text{-}4)$$

where θ_1 is the angle between the Φ,ψ line and a line drawn from r,Φ,ψ to the nearest point on the detector face ($r = d-R$, $\Phi = 0$, $\psi = 0$),

θ_2 is the angle between the Φ,ψ line and a line drawn from r,Φ,ψ to the farthest point on the detector face ($r = d+R$, $\Phi = 0$, $\psi = 0$),

ρ_e is the electron density of the surrounding atmosphere, in electrons/cm^3,

$(d\sigma_e/d\theta)\, d\theta$ is the differential probability per electron that a gamma-ray with original direction $\theta = 0$ will scatter within the differential angle $d\theta$ at mean angle θ in cm^2/electron,

and F is the solid angle subtended by the circular detector face divided by the total solid angle between θ_1 and θ_2.

The F term consists of the detector solid angle model derived and discussed in Sec. 3.1.6 divided by the solid angle between θ_1 and θ_2. It is not discussed

further here. Equation 3.1.1-4 can be approximated well when $\theta_1 - \theta_2$ is small by:

$$P_2 = \pi r_o^2 \sin\theta_a \left(E_s/E_o\right)^2 \left[E_s/E_o + E_o/E_s - \sin^2\theta_a \right] (\theta_1-\theta_2)\, \rho_e\, dr\, F \qquad (3.1.1\text{-}5)$$

where r_o is the classical electron radius, 2.818 x 10^{-13} cm,

θ_a is the arithmetic average of θ_1 and θ_2,

E_s is the scattered photon energy, in Mev

and E_o is the original photon energy, in Mev.

The scattered and original energies are related by

$$E_s = \frac{E_o}{1 + (E_o/0.511)\,(1-\cos\theta_a)} \qquad (3.1.1\text{-}6)$$

The third probability, P_3, is taken as those gamma-rays already described by P_1 and P_2 that are not attenuated as they move from the scattering point at r, Φ, ψ to the detector.

$$P_3 = \exp\left[-\mu_t' \left[s(r,\Phi,\psi) - s_{min}(r,\Phi,\psi)\right] - \mu_w' t_w''\right] \qquad (3.1.1\text{-}7)$$

where μ_t' is the total attenuation coefficient of the atmosphere at gamma-ray energy E_s, in cm^{-1},

μ_w' is the total attenuation coefficient of the space vehicle wall at the gamma-ray energy E_s, in cm^{-1},

$s(r,\Phi,\psi)$ is the distance from the scattering point at r,Φ,ψ to the center of the detector face at $r = d$, $\Phi = 0$, $\psi = 0$, in cm,

$s_{min}(r,\Phi,\psi)$ is the distance from the center of the detector face to the intersection of the outer face of the space vehicle wall along the s line, in cm,

and t''_w is the distance the scattered gamma-ray of energy E_s must travel in the space vehicle wall when traveling along the s line, in cm.

The fourth probability, P_4, is taken as those gamma rays already described by P_1, P_2, and P_3 that give rise to a detectable pulse. This probability is identical to the detector efficiency model that is derived and discussed in Sec. 3.1.5. It is not discussed further here.

The response of the gauge per unit total emission rate, R, is just the integral over all possible limits of the product $P_1P_2P_3P_4$.

$$R = 2 \int_0^{\psi_c} \int_{\Phi_{min}}^{\Phi_{max}} \int_{r_{min}(\Phi,\psi)}^{r_{max}} P_1P_2P_3P_4 \qquad (3.1.1\text{-}8)$$

Keep in mind that P_1 contains the differentials $d\psi$ and $d\Phi$ and P_2 contains the differential dr. A form of Eq. 3.1.1-8 that would look more conventional would be

$$R = 2 \int_0^{\psi_c} \int_{\Phi_{min}}^{\Phi_{max}} \int_{r_{min}(\Phi,\psi)}^{r_{max}} \frac{P_1P_2}{d\psi\ d\Phi\ dr}\ P_3\ P_4\ d\psi\ d\Phi\ dr \qquad (3.1.1\text{-}9)$$

Solutions of Eq. 3.1.1-9 were obtained by programming the finite difference equivalent form for a digital computer. The finite difference form is

$$R \cong 2 \sum_{j=1}^{m} \sum_{k=1}^{n} \sum_{l=1}^{o} (P_1P_2P_3P_4)_{j,k,l} \qquad (3.1.1\text{-}10)$$

where $(P_1P_2P_3P_4)_{j,k,l}$ is the product $P_1P_2P_3P_4$ at the $j^{\underline{th}}$ increment on ψ the $k^{\underline{th}}$ increment on Φ, and the $l^{\underline{th}}$ increment on r; and m,n, and o are the total number of finite difference increments taken on ψ,Φ, and r, respectively.

For the case of the Martian atmosphere where the maximum expected density is quite low compared to that on Earth, the exponential absorption factors in the P_1 and P_3 probabilities due to atmospheric absorption could be neglected. (For the most dense NASA Mars atmosphere model, VM-9, the exponential attenuation on the surface of Mars amounted to less than 5% for a 10 Kev gamma ray and approximately 1% for a 20 Kev gamma ray.) This simplified the model considerably and significantly decreased the amount of computer time required per calculation. These factors could easily be reinserted for calculations involving more dense atmospheres.

The computer program of this model was written in FORTRAN II and run on the Bunker-Ramo 340. A calculation of the response for one set of conditions took from 1 minute to 6 minutes depending on the number of integration increments taken on the r, Φ, and ψ variables.

3.1.2 Wall Streaming Response Model

The earlier studies have determined [3,4] that one of the major sources of noise has been the streaming or multiple scattering of gamma rays down the vehicle skin and into the detector. Consequently, the signal response model described in subsection 3.1.1 was modified to include initial scattering down the wall and subsequent scattering from the wall into the detector.

The significant changes to the model described in Sec. 3.1.1 are: (1) the P_1 probability given by Eq. (3.1.1-1) does not include an attenuation term since the integration on r is done only to the outer surface of the rocket wall, (2) the P_2 probability given by Eq. (3.1.1-4) substitutes a term for ρ_e dr F that describes the fractional amount of the solid angle between θ_1 and θ_2 that is intercepted by the vehicle wall and that includes the electron density of the wall instead of the atmosphere, (3) the P_3 probability is the exponential attenuation of the wall from the original scattering point in the wall at r, Φ and ψ to a point in the wall adjacent to the detector (second scattering point),

(4) the P_4 probability is taken as those gamma rays already described by P_1, P_2 and P_3 that are scattered within the differential distance ds and mean distance s to within the solid angles subtended by the detector (P_4 is identical to P_2 except that the solid angle and differential distance are different. The solid angle is again the F term given in Eq. (3.1.1-4).), and (5) the P_5 probability is again the efficiency or probability that the detector will detect the intercepted gamma ray at the second scatter energy.

The P_4 probability is the most complicated one in this model since at least 4 scattering points for each original scatter point are calculated. A square area of skin 1.5 times the detector diameter was considered for the second scatter points. This area was divided into an even number of smaller square areas of equal size. The center of each of these smaller areas was the second scatter point and was similar to a point source of radiation since it represented the entire area which was used to determine the solid angle subtended between the first and second scatter points. The total contribution was then determined by summing the results from each of the second scatter points. The computer program for this model was written so that either 4 or 16 second scatter points could be assumed. This could be changed if it were found necessary to add more scatter points. However, it was found that changing from 4 to 16 second scatter points did not substantially change the final results but did require more computer time.

The Monte Carlo study discussed in the Introduction for predicting the wall streaming buildup factor resulted in the conclusion that the Monte Carlo technique would be feasible but time did not permit writing a complete Monte Carlo computer code. However, several variance reduction techniques were developed during this work which substantially improved the statistics of this technique. It was originally found that only one gamma ray out of every 10^9 source gamma rays reached the detector. Since this was prohibitively time consuming on a computer, methods of improving the statistics were developed. This work could be developed into a Monte Carlo computer code if desired.

The computer program of this model was again written in FORTRAN II and run on the Bunker-Ramo 340. The computation time was usually less than that of the signal response model because there was only one increment on r. However, there were additional second scatter calculations but the latter calculations were not as time consuming as the former.

3.1.3 Cosmic Radiation Model

One of the sources of radiation that contributes to the noise in a gamma-ray atmospheric density gauge is galactic cosmic radiation. For this model, the cosmic ray spectrum reported by Giannini [7] was used, or extrapolated to include the range of energies applicable for this study. Figure 5.0-1 of Reference 7 gives the cosmic ray spectrum from 1 to 10^{10} Bev. This figure was extrapolated down to 0.010 Mev for this model.

Giannini reported that the cosmic ray flux is believed to be constant between Earth and Mars since the rays originate far outside the solar system. This same assumption was used in the present study.

The equation for the extrapolated cosmic proton intensity spectrum was found to be:

$$N(E) = 8.3 \times 10^{-5} E^{1.283} \text{ particles/cm}^2\text{-sec - Mev} \qquad (3.1.3\text{-}1)$$

where E is cosmic ray energy in Mev.

Then, N(E) dE = number of protons per second with energies in dE about E striking each cm^2 of the detector. This spectrum was normalized to 1 between 10 Kev and 1000 Mev.

Expressed as an equation,

$$\int_{E=0.010}^{E=1000} N(E)\, dE = 1 \qquad (3.1.3\text{-}2)$$

An expression for the range-energy relationship for cosmic protons in the vehicle wall material was obtained by using values from Fig. 3.3 in Chapter 22 of Evans[8] for high energy protons in air. This expression is:

$$r_{air} = 22.2\ E - 107.5 \quad \text{cm} \tag{3.1.3-3}$$

where E is energy in Mev.

The Bragg-Kleeman rule which relates the average range in one absorber to the range in any other absorber gives

$$r_w = 3.2 \times 10^{-4} \frac{\sqrt{A_w}}{\rho_w} r_{air} \tag{3.1.3-4}$$

where A_w is effective atomic weight of wall material

and ρ_w is wall material density, in g/cm^3.

For absorbers other than pure elements, the ratio of the effective atomic weights to the effective stopping power must be used for the A_w term. This is obtained by the following formula:

$$\sqrt{A_w} = \frac{n_1 A_1 + n_2 A_2 + n_3 A_3 + \ldots.}{n_1 \sqrt{A_1} + n_2 \sqrt{A_2} + n_3 \sqrt{A_3} + \ldots} \tag{3.1.3-5}$$

where the n's refer to the atomic fractions of the elements in question.

Substituting the expression for the range in air into Eq. (3.1.3-4) gives

$$r_w = \frac{3.2 \times 10^{-4} \sqrt{A_w}\ [22.2E - 107.5]}{\rho_w} \quad \text{cm} \tag{3.1.3-6}$$

where $\sqrt{A_w}$ is defined by Eq. (3.1.3-5).

The lowest energy E to give a pulse is found by first solving Eq. (3.1.3-6) for E_w (the energy required to pass through the wall) with r_w equal to the wall thickness, t_w. The resulting equation is

$$E_w = \frac{t_w \rho_w}{(22.2)\ (3.2 \times 10^{-4} \sqrt{A_w})} + \frac{107.5}{22.2} \quad \text{Mev} \qquad (3.1.3\text{-}7)$$

where t_w is wall thickness, in cm.

The additional energy required to give a pulse as large as the lower discriminator setting E_ℓ is

$$E_a = E_\ell / y \quad \text{Mev}$$

where y is relative energy efficiency of protons compared to gamma rays

$$y = 5/7.3 = 0.685 \text{ for NaI crystal.}$$

Therefore, the lowest energy proton that will give rise to a pulse is

$$E_{P\ell} = E_a + E_w \,. \qquad (3.1.3\text{-}8)$$

Next, the highest energy that will give a pulse is

$$E_{Pu} = E'_a + E_w \qquad (3.1.3\text{-}9)$$

where E'_a is additional energy required to give a pulse as large as E_u, the upper discriminator setting

or $E'_a = E_u / y$.

Now to get the total number of protons detected

$$N_D = N_c \int_{E_{P\ell}}^{E_{Pu}} N(E)\ dE \quad \text{particles/sec} \qquad (3.1.3\text{-}10)$$

where N_c is total cosmic ray flux, in particles/cm^2/sec. For purposes of this study N_c was assumed to be equal to 2. However, any value other than this may be used readily because this value was read into the computer program for this model. The model was programmed in FORTRAN II and took only fractions of a second on the Bunker-Ramo 340 computer.

3.1.4 Model of Response Directly Transmitted from Source

Another source of background counting rates is the penetration of gamma rays through the tungsten shield placed between the source and the detector. To evaluate this effect the source, shield, and detector configuration shown in Fig. 2-2 was used. This configuration assumed a point isotropic source of radiation and the tungsten shield was divided into two parts.

As stated in Section 2, one of the criterion for optimizing a gamma-ray scatter gauge is minimum shield weight. The shield is divided into two parts to effectively attenuate both the source radiation and scattered radiation with a minimum shield. The source shield which is directly adjacent to the source attenuates the radiation before it has had a chance to spread out or scatter in the atmosphere. Also, as can be seen in Fig. 2-2 shielding placed at this location requires much less volume for a given radius than at any other location. The detector shield attenuates any radiation that may penetrate the side of the detector plus any lower energy radiation that was scattered by vehicle components or in the source shield.

In this model the shield was assumed to be tungsten because of its excellent gamma-ray shielding characteristics and also because this was the shield material in the earlier flight tests. With the known density of tungsten and for any given shield weight, the volume of shielding is just the weight divided by the density. The volume was then divided into two parts for the source and detector shields. A factor or ratio of source volume to total volume determined how the shielding was placed.

The radius of shielding for the source shield is given by

$$r_1 = \frac{4v_1}{Rt} \quad \text{cm} \tag{3.1.4-1}$$

where v_1 is volume of source shield, in cm^3,

R is detector radius, in cm,

and t is detector thickness, in cm.

The width of the detector shield is given by

$$X_3 = \frac{v_2}{Rt} \quad \text{cm} \tag{3.1.4-2}$$

where v_2 is volume of detector shield, in cm^3,

and R and t are as defined above.

The direct transmission through the shields is composed of two parts, attenuation and buildup in the shield. Exponential attenuation in the two shields is given by

$$A_t = e^{-\mu_s (r_1 + X_3)} \tag{3.1.4-3}$$

where A_t is the attenuation factor

μ_s is the total attenuation coefficient of the shield, in cm^{-1},

and r_1 and X_3 are as defined earlier.

The μ_s term is similar to the μ_t term in Eq. (3.1.1-2) and is given by

$$\mu_s = \sigma_s + \tau_s \quad cm^{-1}, \tag{3.1.4-4}$$

where σ_s is the total Compton scattering probability in the shield, in cm^{-1},

and τ_s is the photoelectric effect probability in the shield, in cm^{-1}.

The σ_s term is computed exactly like the Compton scattering probability in (Eq. 3.1.1-2) except that tungsten is used instead of constituents of the atmosphere. The photoelectric effect probability was approximated by the empirical relation

$$\tau_s = a\, E^b \qquad \text{cm}^{-1} \tag{3.1.4-5}$$

where a and b are empirical constants

and E is gamma-ray energy, in Mev.

The constants a and b were determined by taking known values of the photoelectric cross sections at two energies and solving the resulting equations simultaneously. The value for b was determined by using values above the K-edge only. The constant a was found to be 0.3285 and b was -2.42.

The buildup factor was determined by using Chilton's [9] two-parameter formula for point-source buildup factors. This formula has the form

$$B_p = 1 + a_b\, r_b\, e^{b_b r_b} \tag{3.1.4-6}$$

where a_b and b_b are empirical constants

and r_b is the source-detector distance in the medium in mean free paths.

The expression for r_b is

$$r_b = \sigma_s\, X_3 \tag{3.1.4-7}$$

where σ_s is again the total Compton scattering probability, in cm^{-1},

and X_3 is thickness of detector shield, in cm.

The earlier experiments [4] have shown that the only energies that are not completely attenuated by the shield are the ones from high energy contaminants. Consequently, the energies used in this model were from 0.7 Mev up to approximately 1.3 Mev. Therefore, the photoelectric effect did not enter into this calculation. Also,

because of the small thickness of source shield, the detector shield was the only one used for the buildup part of the computation. The values for a and b were taken from Chilton's article at 0.5 Mev for tungsten. This was assumed to be the most representative energy for the contaminants.

The direct transmission was then found to be a combination of the attenuation factor, buildup factor, source strength, and the solid angle. Expressed as an equation

$$D_1 = B_p A_t S A_b \frac{tR}{(2\pi D^2)} \quad \text{counts/sec.} \qquad (3.1.4\text{-}8)$$

where B_p is buildup factor defined by Eq. (3.1.4-6),

A_t is attenuation factor defined by (3.1.4-3),

S is source strength, in disintegrations/sec,

t is detector thickness, in cm,

R is detector radius, in cm,

D is source-detector distance, in cm,

and A_b is abundance of the contaminant energy.

This model was programmed in FORTRAN II and run on the Bunker-Ramo 340 computer. A set of computations took only fractions of a second.

3.1.5 Detector Efficiency Model

In the earlier discussions of the signal response model and wall streaming response model the final probabilities, P_4 and P_5, respectively, were seen to be the detector efficiency or the probability that the gamma ray which intercepts the detector will give rise to a measured pulse. This probability is a function of the detector size and material, the gamma-ray energy, and the discriminator settings on the electronics used to process the pulses from the detector. For a given detector with fixed discriminator settings, this probability which will be called P_5 here is given by:

$$P_5 = f(E) \qquad (3.1.5\text{-}1)$$

where f(E) is a function of the gamma-ray energy.

Since the primary interest in this program is in the use of scintillating crystals for detection, a generalized form of f(E) was derived for this case. For a more detailed discussion of this model see Appendix A.

3.1.6 Detector Solid Angle Model

The detector in the signal response and wall streaming response models was assumed to be a right cylindrical NaI (Tl) crystal. The circular detector face subtended a solid angle which depended on the location of the detector in relation to the scattered gamma rays. This physically corresponded to determining the fractional number of gamma rays emitted from a point source that was intercepted by the circular face of the detector.

Zumwalt [11] treated this situation, but it was found that his series solution did not converge rapidly for all detector positions. Consequently, an alternate series solution that did converge rapidly for all detector positions was developed. This alternate solution was easily programmed for a digital computer. For a detailed discussion of this model see Appendix B.

The model discussed in Appendix B represented part of the F term in Eq. (3.1.1-4) and the equivalent equation in the wall streaming response model. The remaining part of F was the total solid angle between the θ_1 and θ_2 angles as defined in Eq. (3.1.1-4). Therefore F can be expressed as:

$$F = \frac{\Omega}{2\pi (\cos \theta_1 - \cos \theta_2)} \qquad (3.1.6\text{-}1)$$

where Ω is given by Eq. (B-5)

and θ_1 and θ_2 are as defined in Eq. (3.1.1-4).

3.2 Model Predictions

In this section model predictions for signal and wall streaming gauge responses are presented for comparison with the two-dimensional results obtained previously. The purpose of obtaining these predictions is to determine if the three-dimensional models are accurate and to determine if any significant differences between these models and the two-dimensional ones exist. To accomplish these two objectives the following predictions have been made: (1) signal response to atmospheric density, (2) signal response as a function of scattering distance, (3) signal response to variations in atmospheric composition, (4) signal response to shock wave density perturbations, and (5) signal and wall streaming response to two wall materials and thicknesses as a function of gamma-ray source energy. Unless otherwise stated the gauge dimensions used in the predictions are those listed in Table 3-2 which are those expected for the Mars atmosphere density sensor.

3.2.1 Signal Response to Atmospheric Density

The response of the signal predicted by the model outlined in Section 3.1.1 for the gauge dimensions given in Table 3-2 is linear with atmospheric density over the maximum range of atmospheric densities expected on the surface of Mars. This is obviously true since the attenuation of the gamma rays for this atmospheric density range could be neglected (see Section 3.1.1). The predicted signal responses as a function of altitude for NASA Models VM-8 and VM-9 are given in Fig. 3-3 for a source energy of 100 Kev and discriminator settings of 65 and 115 Kev. These two models represent the maximum and minimum densities expected on the surface of Mars. The atmospheric densities of these models as a function of altitude are given in Fig. 3-4.

The fact that the predicted gauge response is linear with atmospheric density allows one to significantly reduce the number of model

calculations that are necessary in the study of the gamma-ray technique. The result obtained at one density is easily converted to that at any other density in the range of interest by multiplying by the ratio of the desired density to that used in the calculation.

3.2.2 Signal Response as a Function of Distance from Sensor

To illustrate the effective sample volume of the gamma-ray scatter gauge, the response as a function of distance from the source has been calculated. Figures 3-5A and 3-5B give the number of gamma rays that are scattered from any point and are eventually detected out of 10,000 total gamma rays detected. The gauge parameters used in this calculation are those given in Table 3-2 with a source energy of 100 Kev, a detector efficiency equal to the total efficiency of a 2" x 2" NaI(Tl) crystal, and an atmospheric density of 2×10^{-5} g/cm^3.

The maximum number of gamma rays detected are at a distance of about 120 cm and the number detected approach zero asymptotically as distance is increased. Since there is negligible attenuation by the atmosphere for the density range of interest on the surface of Mars, the response as a function of distance shown in Figs. 3-5A and 3-5B is independent of density. The response as a function of distance would be expected to vary only slightly with other parameters such as source-to-detector distance, source energy, and detector discriminator settings.

3.2.3 Signal Response to Variations in Atmospheric Composition

Previous studies [3] indicated that the response of the gamma-ray scatter gauge is affected significantly by variations in atmospheric composition at a density equal to that at sea level on Earth when gamma-ray energies less than about 100 Kev are employed. This effect is due to variations in the attenuation of atmospheres of different composition which is caused primarily by variations in the photoelectric effect interaction (complete absorption). Since the atmospheric density likely to be encountered on Mars is much lower than that on Earth by a factor of about 50, gamma-ray attenuation by the atmosphere can be neglected. This

means that there is no variation in gamma-ray scatter gauge response except that small amount due to the slight variation in the ratio of atomic number to atomic mass (Z/A).

In the case of the Mars atmosphere, this variation is at a maximum value for the largest variation of argon percentage in the atmosphere since the Z/A ratio for argon is most different from the other elements likely to be found in the Mars atmosphere. The maximum effect is obtained by considering the response to the NASA Model VM-6 Mars atmosphere in comparison to the NASA Model VM-8 at the same densities. The difference between the two responses is 3.2% which is just the difference in the average Z/A ratio. This is the maximum effect to be expected in atmospheric density measurements on the surface of Mars.

3.2.4 Signal Response to Density Variations Induced by Shock Waves

The response of the gamma-ray backscatter gauge to shock wave density perturbations was determined by using the signal response model to calculate the response for two hypothetical shock waves representing the maximum shock wave perturbation at two atmospheric density extremes. These responses are compared to the response predicted when no shock wave is present. The density change of the hypothetical shock waves was assumed to be of uniform thickness above the spacecraft outer wall and of uniform density. For the low density case (atmospheric density = 1.8×10^{-7} g/cm^3) the shock wave standoff distance was taken as 24 cm and the density behind a shock wave was taken as 1.1×10^{-6} g/cm^3 or 6.0 times higher than the ambient density. For the high density case (atmospheric density = 2.6×10^{-5} g/cm^3) the shock wave standoff distance was taken as 120 cm and the density behind the shock wave was taken as 1.0×10^{-4} g/cm^3 or 3.86 times higher than the ambient density. The gauge parameters are as shown in Table 3-2 with a source energy of 100 Kev and upper and lower discriminator settings of 115 and 65 Kev, respectively.

Three different source collimation angles were employed in the calculations to study the effect of collimation on the variation of response induced by shock wave density perturbations. The results of these calculations are given in Table 3-4. They indicate that the effect of the shock wave density perturbations is very significant for both hypothetical shock waves. They also indicate that collimation of the source is somewhat effective in minimizing this effect. However, a significant amount of total response is lost when collimation is employed.

By stringently collimating both the source and detector so that only gamma rays that scattered from outside of the shock wave could be detected, one could (theoretically) completely eliminate the effect of shock wave density perturbations. This is only true for atmospheric densities low enough so that one may neglect attenuation, such as is the case on the surface of Mars. However, such stringent collimation could only be accomplished with very large attendant losses of total signal and with much heavier collimation shielding. An alternate method of eliminating this effect might be to use two gauges simultaneously or to use the mathematical models developed here in conjunction with other data known about the entry path of the spacecraft.

3.2.5 Signal and Wall Streaming Response as a Function of Source Energy

Since the signal response is independent of atmospheric attenuation it depends primarily on the Compton scattering cross section for a given gauge configuration. The variation of the signal response as a function of source energy is shown in Fig. 3-6. The signal responses given are for the gauge parameters given in Table 3-2 with the detector efficiency taken as the total efficiency of a 2" x 2" NaI(Tl) crystal and the NASA Model VM-6 Mars atmosphere with a density of 1.8×10^{-7} g/cm^3. These calculations are for the phenolic spacecraft wall described in Table 3-2. The results are listed in Table 3-5.

The wall streaming response depends strongly on attenuation down the spacecraft wall and on the wall thickness available for scattering. Therefore,

the wall streaming response depends on the material composition, density, and thickness of the spacecraft wall. Calculations for the wall streaming for the two spacecraft walls described in Table 3-2 for the gauge parameters used in calculating the signal response are listed in Table 3-6. The results for the phenolic wall are plotted in Fig. 3-6 for comparison to the signal response.

It is seen that the predicted signal response increases monotonically with decreasing source energy down to 10 Kev while the predicted wall streaming response exhibits a maximum value at a source energy of about 1 Mev. This seems to indicate that for a maximum signal-to-noise ratio, one would pick a source energy as low as possible. However, it should be pointed out that there are several complicating circumstances to this conclusion. One is that no discriminator settings are used in these calculations, so it is not possible to ascertain the effect that optimizing the discriminator settings would have on the signal-to-noise ratio. Another consideration is that wall streaming is not the sole source of noise. These factors are all highly interdependent and point out the need for a multivariable search routine in optimizing the gauge configuration. It is shown later in Section 4 that an optimum source energy occurs at 76 or 110 Kev depending upon the source-to-detector distance and other gauge parameters chosen.

3.3 Summary Discussion of Model Predictions

The three-dimensional model predictions given here are consistent with the two-dimensional models previously derived [3] and experimentally verified [4]. These models must be assumed to be accurate based on this comparison. The primary difference between these results and those obtained previously is due to the different atmospheric density ranges being considered. In the present case the maximum expected atmospheric density on Mars is about 50 times less dense than that at sea level on Earth. This means that the attenuation of gamma rays to and from the scattering point is negligible for a Mars atmospheric density sensor. This means that the effect of atmospheric composition variations will be small.

The most serious problem area indicated by calculations with the three-dimensional models is the effect of density perturbations caused by shock waves. Since attenuation is negligible in the density range of interest on Mars, one could theoretically eliminate this effect by extreme collimation of the source and detector. However, this amount of collimation would require greater shield weights and a considerable loss of total signal. Two possibilities exist for eliminating this effect other than by collimation: (1) the simultaneous use of two gauges with different collimation designs and (2) the use of the mathematical models developed here with additional information on the spacecraft entry path to correct the effect by computation. These techniques have not been studied as yet.

When discriminators are not employed and the controlling source of noise is assumed to be wall streaming, the maximum signal-to-noise ratio would be obtained at the lowest possible gamma-ray source energy. This simple analysis neglects two important considerations. These are that the results of the analysis change when: (1) optimum discriminator settings are employed, and (2) wall streaming is not the controlling source of noise. An optimum source energy of 76 or 110 Kev is found by the search routine described in Section 4. This result demonstrates the need for a multivariable search routine capable of handling the complex interrelationships of the parameters involved in optimizing the gamma-ray sensor design.

A description of a master computer program to optimize the design of a Mars atmosphere gauge and the results of the optimization design are given in the next section.

4. MULTIVARIABLE SEARCH ROUTINE

The final objective of the present study was to use computer programs to optimize a gauge for installation on a Mars atmosphere gauge. In a design optimization, the design arrangement must be the first thing chosen. For this case this arrangement was dictated by the Mars atmosphere gauge configuration. Secondly, the proper function to be maximized (or minimized) must be selected. This was obviously the signal-to-noise ratio for the gamma gauge.

Since there must be a marriage between the mathematical models and the optimization technique, the choice of technique must be kept in mind while the modeling is in progress. A small change in the model may permit use of a quicker or more efficient optimization technique. For this study the Rosenbrock[5] technique for finding the greatest or least value of a function of several variables was used. This technique and the master computer program for combining it with the three-dimensional models are discussed in this section. The three-dimensional models for signal and noise were discussed in Section 3 and therefore are not discussed further here.

4.1. Master Optimization Program

The master computer program for optimizing the atmospheric density gauge consisted of an input program, a setup subroutine for calling the Rosenbrock search, the Rosenbrock subroutine, a subroutine called by the Rosenbrock that contains the function to be minimized, and subroutines for calculating the basic signal, wall streaming, cosmic rays, direct transmission, efficiency, and one of the solid angles subtended. These latter six subroutines were described in Section 3. The relation of these subroutines and program to effect an optimization can be explained best by again examining the schematic diagram of general mathematical model optimizations shown in Fig. 2-1.

The constraints shown as (1) in the figure dictated the model arrangements for certain cases and in others, controlling dimensions such as the source-to-detector distance, gamma-ray energy, and minimum and maximum collimation

angles in two planes were read into the input program. The setup subroutine determined which parameters were adjustable for the case under consideration. This is represented by (2) in Fig. 2-1. The Rosenbrock subroutine which is the search routine of Fig. 2-1 was then called. This subroutine then used the subroutine that contained the function to be minimized, or the value of criterion in Fig. 2-1. The mathematical models, (3) in Fig. 2-1, were used by the value of criterion subroutine to calculate each of the sources of noise. The noise was then determined by summing the cosmic, direct, and wall streaming responses and the ratio of this value to the signal was computed. This criterion was then compared with the previous value and if it were smaller, the parameters were adjusted further in the same manner as originally and the procedure was duplicated. This procedure was continued until the new criterion was larger than the previous one or until the noise-to-signal ratio became negative which of course was physically impossible. If the criterion were larger than the previous one, the program adjusted the parameters in the opposite manner to effect a lower criterion. The details of the adjustment of parameters and their limiting values are discussed in subsection 4.2.

For this study, nine variables were originally considered for optimization. These variables were source-to-detector distance, detector radius and thickness, upper and lower discriminator settings on the electronics, gamma-ray energy, and minimum and maximum collimation angles in two planes. Later, it was found that certain variables such as the collimation angles, detector size, and gamma-ray energy were essentially fixed by design considerations. One example of this principle was the selection of a radiation source which automatically determined the gamma-ray energy. Gamma-ray energy, the presence of high-energy contaminants, ease of manufacture, and cost were a few considerations that determined which sources would be used. The most likely candidates were found to be Gd^{153} or Eu^{155} which both emit low gamma-ray energies. Thus one of the adjustable

parameters was eliminated by this source selection. Reducing the number of adjustable parameters simplified the computer program substantially because each of the parameters was adjusted one at a time. The details of the Rosenbrock technique and its manner of adjusting these parameters are given in the following subsection.

After the parameters were adjusted until a minimum value of criterion was found, the program selected the optimum values of parameters, (6) in Fig. 2-1, which were the output of the program. These optimum parameters were used to effect the optimum gauge for each of several different designs. In addition to the optimized variables, certain other parameters such as shield weight, atmospheric composition, and vehicle skin materials had to be studied to optimize the gauge design. Shield weights of 500, 1000, and 2000 grams were used to determine the optimum design for each weight and from this the optimum weight. Atmospheric composition and density were also varied in an effort to determine their effect on an optimum gauge. Thus, for each fixed parameter, an optimum design was determined and an examination of the various designs should determine the best parameters to use.

4.2 Rosenbrock Search Technique

The search routine that was used in the optimization program was the automatic method of finding the greatest or least value of a function due to Rosenbrock [5]. This technique was developed for use on a digital computer and arose from a need to design chemical processes so that they produce the most economical result. During the development of this work, Rosenbrock states that over fifty different programs were run. The technique was incorporated into a program for Mercury.

The primary merit of this technique is that of orthogonalizing the space and rotating the coordinates of the search to line up with a ridge. This procedure eliminates most of the interactions between the design parameters and effects excellent ridge following.

The parameters are changed in turn, reducing the value of criterion as far as possible with each variable and then passing on to the next. The length of step to be taken in any desired direction, assuming this direction to be known, was decided arbitrarily to be e. If this resulted in a success (i.e., lower minimum) e was multiplied by $\alpha > 1$. If it failed, e was multiplied by a value $-\beta$ where $0 < \beta < 1$. Therefore if e were initially so small that it made no change in the criterion, it was increased on the next attempt. Each of the attempts will be called a "trial".

The next problem was to decide when and how to change the directions in which the steps e are taken. It was necessary to examine neighboring points in each of n directions, in order to determine which is the best direction to advance. In this technique it was decided to make one trial, of the kind described above, in each of the n directions in turn. The method for determining the point at which to compute new directions was to go on until at least one trial had been successful in each direction, and one had failed.

The values for α and β were determined by making a set of calculations of 200 trials. Rosenbrock states that too great refinement is not justified since the results must depend to some extent on the particular problem. Values of $\alpha = 3$ and $\beta = 0.5$ were originally tried; however, it was found that other values effected a quicker convergence so that the final values used here were $\alpha = 5$ and $\beta = 0.3$.

One of the major problems in the Rosenbrock method is in the application of limits on the real variables. This is shared with all methods which use a transformed space. Rosenbrock recognized this difficulty and attempted to overcome it by applying penalty factors. These penalty factors created other difficulties which are not easily overcome.

The answer appears to be that limits must be tested and used in the space where they apply. Any move that causes the criterion to exceed a preset limiting value is an automatic failure. This technique has been used successfully with other

search techniques, provides absolute bounding of the problem space, and eliminates a computation of the performance index for each move which exceeds a boundary.

In the course of the present study, limits originally were put on several of the variables. However, it was found that the computer would try another direction and keep returning to the limits. Consequently, it would continue to go around this "loop" and would never output optimum parameters. This was handled by removing the limits from the variables and letting the computer find the optimum value regardless of its value. Then it was examined and if it were physically impractical, this parameter was "fixed" and the computer was then allowed to search on the remaining variables.

An example of this exceeding of practical limits can be seen in Table 4-1 where the source-to-detector distance was approximately 554 cm. This was because of the low density wall material which resulted in a high wall streaming response. Therefore to reduce this streaming response and effect a minimum noise-to-signal ratio the program pushed the source-to-detector distance variable to the large 554 cm value. The maximum allowable was stated by NASA to be 50 to 150 cm so the variable was fixed at each of 50, 100, and 150 cm and the search was made on the remaining variables.

The other major limit that was imposed in this study was to require the noise-to-signal ratio to remain positive. If this ratio became negative (which it did if the direction tried was effecting smaller minimums) the program was terminated. This is one of the weaknesses of this study and could be overcome by going back and changing the values of α and β to find more optimum results. The number of "trials" that were made in each of the design cases varied, but usually was around 25.

Another limitation of the Rosenbrock as with many other search routines is that a function with only one maximum or minimum can be accurately optimized. Points of inflection will result as the optimum value if the technique finds one. Therefore the technique should be used only for smooth functions. One way of checking to see if the "minimum" or "maximum," is truly the real one is to start

the variables at a low value and then at a high value. If they both converge to the same point the result is accepted as a true minimum or maximum.

4.3 Optimization Results

As stated in Section 4.1 certain gauge parameters were found to be fixed by spacecraft design considerations or by state-of-the-art development of the gauge components. Included in this category are: spacecraft wall material and thickness, total gauge weight and volume, the use of scintillation crystal-photomultiplier detectors, and gauge performance characteristics such as required response time and accuracy. The variable gauge design parameters that remain include: (1) distance of source and detector from the wall, (2) source intensity, (3) detector material, (4) detector diameter, (5) source collimation angles, (6) detector collimation angles, (7) shield weight, (8) detector thickness, (9) source energy, (10) source-to-detector distance, (11) lower discriminator setting, and (12) upper discriminator setting.

Theoretically, one could search all of these twelve gauge design parameters for the optimum gauge design. However, searching on twelve parameters with the complexity of the mathematical models described in Section 3.1 would require an inordinate amount of computer time. Some of the twelve gauge design parameters are intuitively known to have only a slight effect on the gauge performance and others are constrained by other practical limitations.

The first five of the twelve variable gauge design parameters were fixed since they were not expected to significantly affect the gauge performance. The distance of the source and detector to the spacecraft wall was fixed at 5 cm. Increases in the source intensity would obviously improve the gauge performance up to the point that the noise level is controlled by the source intensity. A reasonable source intensity for the Mars atmospheric measurement appears to be 20 curies. Therefore, the source intensity was fixed at this value. The scintillation detector material was assumed to be NaI(Tl). For this study increases

in detector diameter would tend to increase both the signal and the noise by proportionate amounts. Therefore, the detector diameter was fixed at 4 inches. The detector collimation angles would be expected to affect the gauge performance, but the amount of shielding necessary to accomplish any significant amount of collimation would probably be prohibitive. Therefore, the detector was left uncollimated for all predictions.

The effect of the next two gauge design parameters, detector collimation and shield weight, can easily be examined by taking several discrete values of each. It is useful to also examine wall material and thickness in this same way. Even though these two parameters are fixed by the spacecraft design, the particular design of the spacecraft wall (lamination of a thickness of phenolic heat shield and a thickness of aluminum structure) could not be easily incorporated into the mathematical models. It was therefore decided to examine the laminated thicknesses separately to determine the effect of each lamination. Hopefully, one or the other would control the gauge response or the gauge response would not be seriously affected by the spacecraft wall.

This leaves five gauge design parameters that should be optimized. These are:

detector thickness

source energy

source-to-detector distance

lower discriminator setting

upper discriminator setting

The first series of computer runs held source energy constant at 100 Kev (this value is appropriate to ^{153}Gd) and searched on the remaining four parameters for various fixed values of wall material (phenolic or aluminum), wall thickness (.3175 cm of aluminum, 0.762 cm of phenolic, and 1.08 cm of phenolic), shield weight (2000, 1000, and 500 grams), and source collimation angles ($\pm 45^{\circ}$ and $\pm 30^{\circ}$). The criterion for optimum gauge performance used was the minimum noise-to-signal ratio. The results of this series of runs are given in Table 4-1.

It became obvious in making this series of optimization runs that there are two major disadvantages inherent to the Rosenbrock search routine for this particular application. First of all, there are no limits on the variables being searched so negative values are allowed. Secondly, the minimum values found depended upon: (1) the search order, (2) the initial values given for each variable, and (3) the values for α and β which control the step size. To combat these two problems and insure that the correct minima were being obtained, the same search was made several times and the search order, initial values given, and α and β values were varied each time. The noise-to-signal ratio was printed out each time and one could judge the best minimum value by examining this ratio for each individual step. In this way negative values of the parameters could be ignored. One modification of the program was made. This consisted of terminating the search when a negative value was obtained.

In making the series of runs listed in Table 4-1 it was found that the noise-to-signal ratio was quite insensitive to detector thickness. Detector thicknesses of 0.6 cm or 1.6 cm gave the same noise-to-signal ratio to within $\pm$ 2%. Therefore, in future runs this parameter was fixed at 0.6350 cm (1/4 inch).

The next interesting fact is that the direct transmission of gamma rays is a negligible source of noise for all shield weights tried. In all cases where the spacecraft wall material is phenolic resin, the source-to-detector distance was increased to very large values to make the streaming of gamma rays down the spacecraft wall negligible in relation to the amount of cosmic radiation detected. When an aluminum wall was used the source-to-detector distance required to accomplish this was decreased by an order of magnitude. This indicates that the controlling wall material is the layer of phenolic resin. Therefore, subsequent runs used one of two fixed values of phenolic wall thickness: 0.762 or 1.08 cm.

The effect of changing the collimation angles on the noise-to-signal ratio was relatively small. The signal response is almost directly proportional

to the total solid angle allowed by the collimation angles. The collimation angles have about the same effect on the streaming of gamma rays down the spacecraft wall. However, since this is a negligible source of noise in the present series of runs, the collimation angles do not affect the total noise. In subsequent runs the collimation angles were fixed at $\pm 45^{o}$.

The optimum source-to-detector distances obtained were not compatible with limitations imposed by the spacecraft design and so three fixed realistic values of this parameter were used in subsequent runs to examine the effect of this parameter.

The first series of runs did not determine optimum source energy. It is possible that the theoretical optimum source energy could be significantly different from the ^{153}Gd source with an average energy of 100 Kev. The next series of runs was designed to determine the optimum source energy and corresponding lower and upper discriminator settings for various fixed values of the parameters that were found to be important in the first series of runs. These fixed values of importance were source-to-detector distances of 150, 100, and 50 cm; shield weights of 2000, 1000, and 500 grams; phenolic resin wall thicknesses of 0.762 and 1.08 cm; and detector thickness of 0.6350 cm. The results of this series of runs are given in Table 4-2.

In this second series of runs the controlling source of noise is the streaming of gamma rays down the spacecraft wall. This is the case because three, small fixed values of the source-to-detector distance have been employed in this series of runs. For the source-to-detector distance of 150 cm, the optimum source energy is 76.3 Kev while the optimum source energy is 110 Kev for the two smaller source-to-detector distances of 100 and 50 cm. These results indicate that the 100 Kev energy of the ^{153}Gd source is very near optimum. It is interesting to note that the optimum energy one would obtain by considering only

the signal response and noise response with no discriminator settings would be at about 15 Kev or less.

There are two problems associated with these first two series of runs that needed some further investigation. Probably the most important was that the noise level due to phenomena other than the source-generated noise seemed too low. Recall that the cosmic radiation background response was assumed to be controlling in this general area of noise. Other sources of noise in this same category would be electronic (primarily thermal emission at the photocathode) and natural radioactivity in the surroundings. Both of these sources of noise, like cosmic radiation, would be independent of the radioisotope source being used and, therefore, independent of the source-to-detector distance.

The hypothesis that the non-source generated noise level is too low can only be eventually determined by experimental results. However, the effect of a higher noise level in this category can be ascertained by simply assuming a much higher cosmic radiation flux. This means that a higher noise level by any source of radiation in this category is being simulated by increasing the noise contribution of the cosmic radiation. To accomplish this, the assumed particle flux was changed from 2 to 12,350 protons per cm^2 per second. This value of 12,350 was established by obtaining the value required to obtain 30 counts per second for discriminator settings of 0 and 2.5 Mev with the 0.6350 cm thick, 4 inch diameter NaI(Tl) detector.

The other problem is a conceptual one. It is probable that the noise-to-signal ratio is not the best characteristic to minimize as a criterion for the optimum gauge performance. Probably a better characteristic is the variance of the atmospheric density measurement. This parameter is given by:

$$\sigma^2(\rho) = \left(\frac{d\rho}{dR}\right)^2 \sigma^2(R) \qquad (4.3\text{-}1)$$

where $\sigma^2(\rho)$ is the variance of the atmospheric density measurement, $d\rho/dR$ is the slope of the calibration curve, and $\sigma^2(R)$ is the variance of the measured counting

rate. This last parameter is taken as:

$$\sigma^2 (R) = \sigma_G^2 (R) + \sigma_B^2 (R) \qquad (4.3\text{-}2)$$

where σ_G^2 (R) is the variance of the gross counting rate and σ_B^2 (R) is the variance of the background counting rate. These component variances are taken as due solely to the normal statistical fluctuations of signal and background (noise) for a fixed observation time. Therefore, they represent the minimum attainable variances. They are given by:

$$\sigma_G^2 (R) = R_G \qquad (4.3\text{-}3)$$

$$\sigma_B^2 (R) = R_B \qquad (4.3\text{-}4)$$

where R_G is the gross counting rate (signal plus background) and R_B is the background counting rate or noise. Since the high-altitude accuracy is of most interest and is most crucial, σ_G^2 (R) is taken as R_B and σ^2(R) becomes 2 R_B. (Note: Other sources of error could be included here if desirable. For example, the error due to shock-wave density perturbations could be included here. This is not done here, since it is beyond the scope of the present contract.)

With these two changes a search of the four parameters source energy, source-to-detector distance, lower discriminator setting, and upper discriminator setting was made. The results of this search are given in Table 4-3. Note that the source-to-detector distance is reduced over the previous runs by a factor of about two. This indicates that the level of the non-source generated noise level has a significant effect on the optimum source-to-detector distance. When experimental results are obtained on this noise level, more realistic optimum values can probably be obtained for the source-to-detector distance.

The advantage of searching for a minimum variance is that the best possible measurement accuracy is directly obtained since only the error due to

statistical source fluctuations is considered. The measurement standard deviation is just the square root of the variance.

Since the optimum source energy found was 106.4 Kev, the ^{153}Gd source with an average energy of 100 Kev should give quite good results. This was checked with one final run fixing the source energy at 100 Kev and searching on the three parameters source-to-detector distance and upper and lower discriminator settings. The results of this run are given in Table 4-4 and indicate that, as expected, the source energy of 100 Kev is essentially as good as the optimum of 106.4 Kev found by the search routine.

4.4 Discussion of Results and Conclusions

The results of the optimization study indicate that this is a very promising method of optimizing the gamma-ray atmospheric density sensor. When experimental results become available so that realistic noise levels can be established, the method should prove to be even more helpful in exactly establishing the optimum design parameters. At this time further optimization studies should await the experimental results necessary to establish the levels of the various sources of noise.

The major findings of this study were: (1) optimum gauge performance was quite insensitive to detector thickness, (2) the direct transmission of gamma rays was a negligible source of noise under all conditions considered here, (3) the material controlling the streaming of gamma rays down the spacecraft wall was the low density phenolic heatshield for all conditions considered in this study, (4) the effect of varying the collimation angles on the source was about what would be predicted by taking the signal response as directly proportional to the total solid angle subtended by the collimation angles, (5) the optimum source energy for all conditions considered here was about 100 Kev, (6) the effect of the non-source generated noise level on the optimum source-to-detector distance was quite significant, (7) the optimum discriminator settings vary from 65 to

106 Kev, and (8) the optimum gauge design gives a measurement standard deviation of 0.530×10^{-8} g/cm^3.

5. REFERENCES

1. D. B. Hakewessel, "Air Density Sensor ADS-103 Design and Operation," Final Report on NASA Contract No. NAS1-4349, August 1965.

2. D. B. Hakewessel, "Feasibility Study for an X-ray Backscatter Free Air Density Sensor," NASA Contractor Report No. 66148, Sept. 1966.

3. R. P. Gardner and D. R. Whitaker, "A Theoretical Study of the Gamma-Ray Scattering Technique for Measuring Atmospheric Density," NASA Contractor Report No. 66142, Aug. 1966.

4. R. P. Gardner and D. R. Whitaker, "Experimental Verification of Gamma-Ray Atmospheric Density Sensor Mathematical Model Predictions," NASA Contractor Report No. 66476, Aug. 1967.

5. H. H. Rosenbrock, "An Automatic Method for Finding the Greatest or Least Value of a Function," Computer Journal, Vol. 3, pp. 175-184, October 1960.

6. N. W. Gebbie., Final Report - Mars Probe Lander Density Sensing System, NASA CR-66094, Feb. 1966.

7. N. W. Gebbie , Final Report - Mars Probe Lander Density Sensing System, Appendix A, NASA CR-66094, Feb. 1966.

8. Evans, R. D., The Atomic Nucleus, McGraw - Hill Book Company, Inc., New York, 1955.

9. A. B. Chilton, "Two-Parameter Formula for Point-Source Buildup Factors," Nucleonics, Vol. 23, No. 8, p. 119, Aug. 1965.

10. C. E. Crouthamel, Applied Gamma-Ray Spectrometry, Pergammon Press, New York, 1960.

11. L. R. Zumwalt, "Absolute Beta Counting Using End-Window Geiger-Mueller Counters and Experimental Data on Beta-Particle Scattering Effects, Appendix B: The Solid Angle Subtended by a Circular Disk," AECU-567, Oak Ridge National Laboratory, Oak Ridge, Tennessee, March 13, 1950.

FIGURES

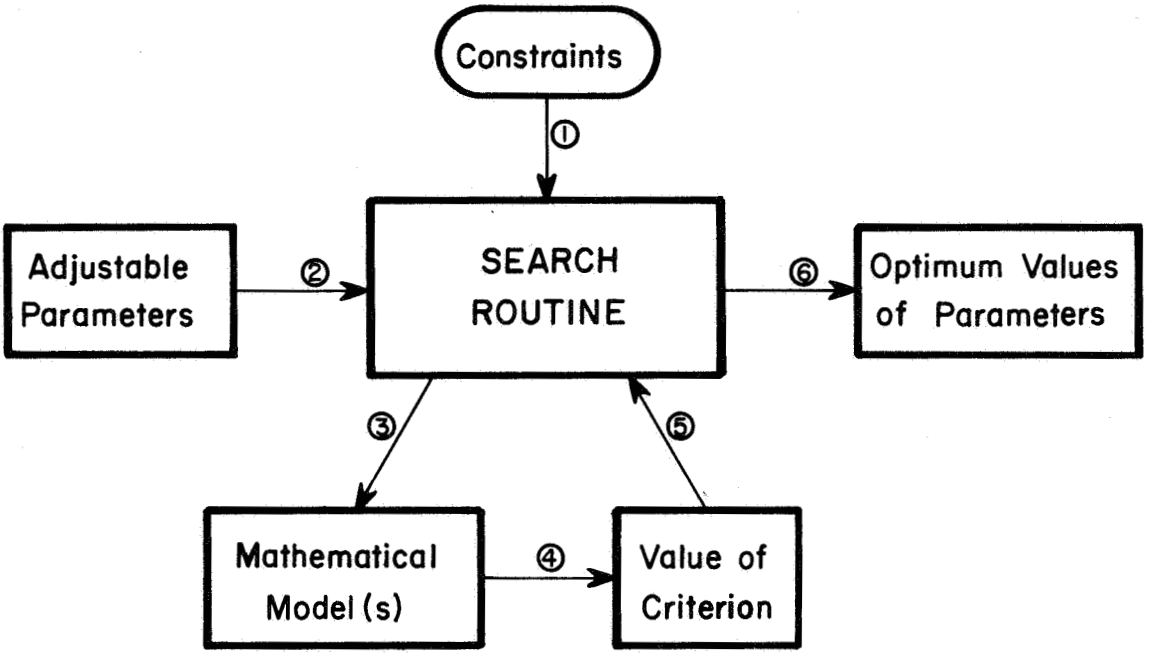

Fig. 2-1 Schematic diagram of mathematical model optimization procedure

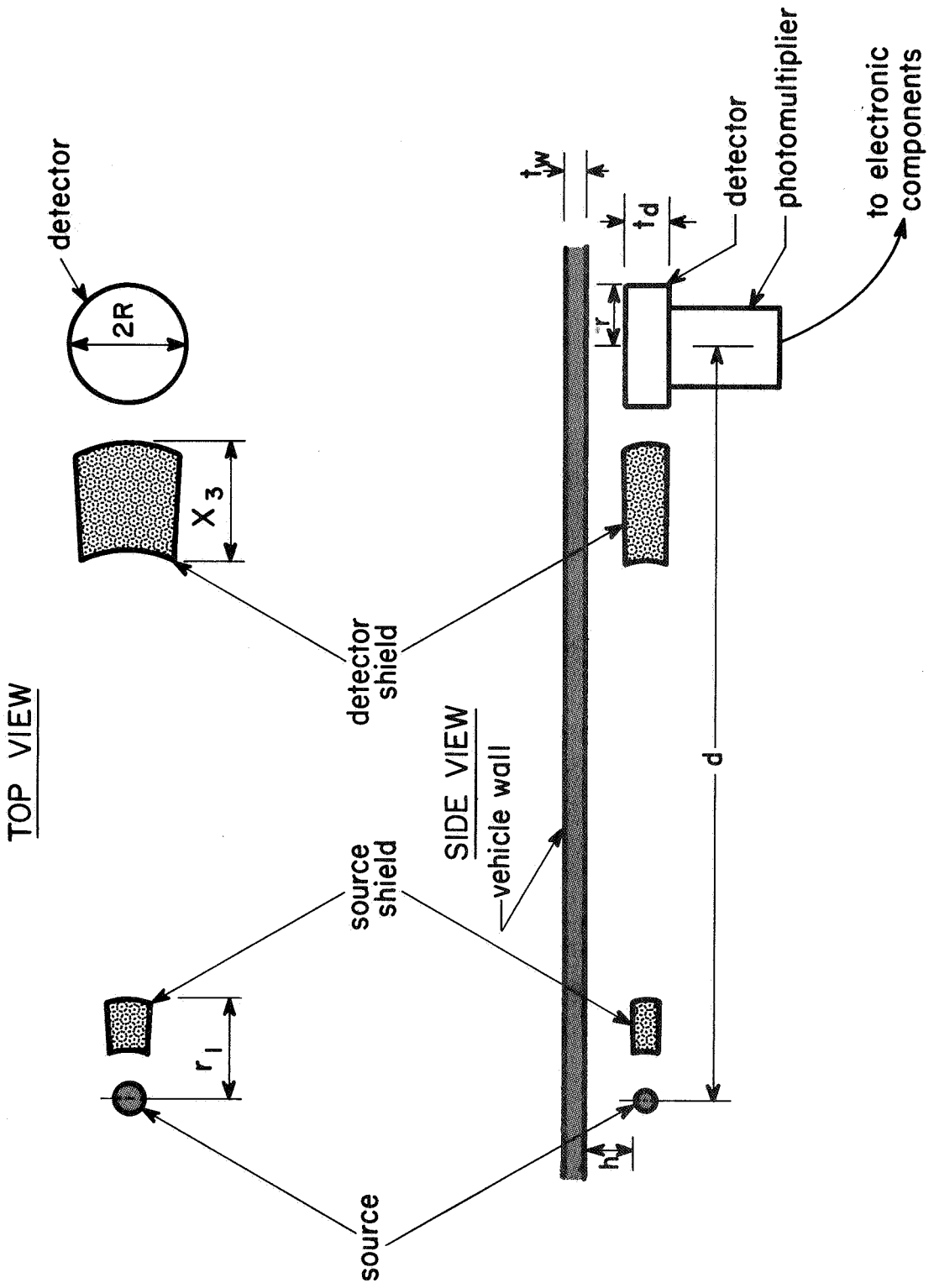

Fig. 2-2 Schematic diagram of the gamma-ray scatter gauge for the measurement of the Mars atmospheric density

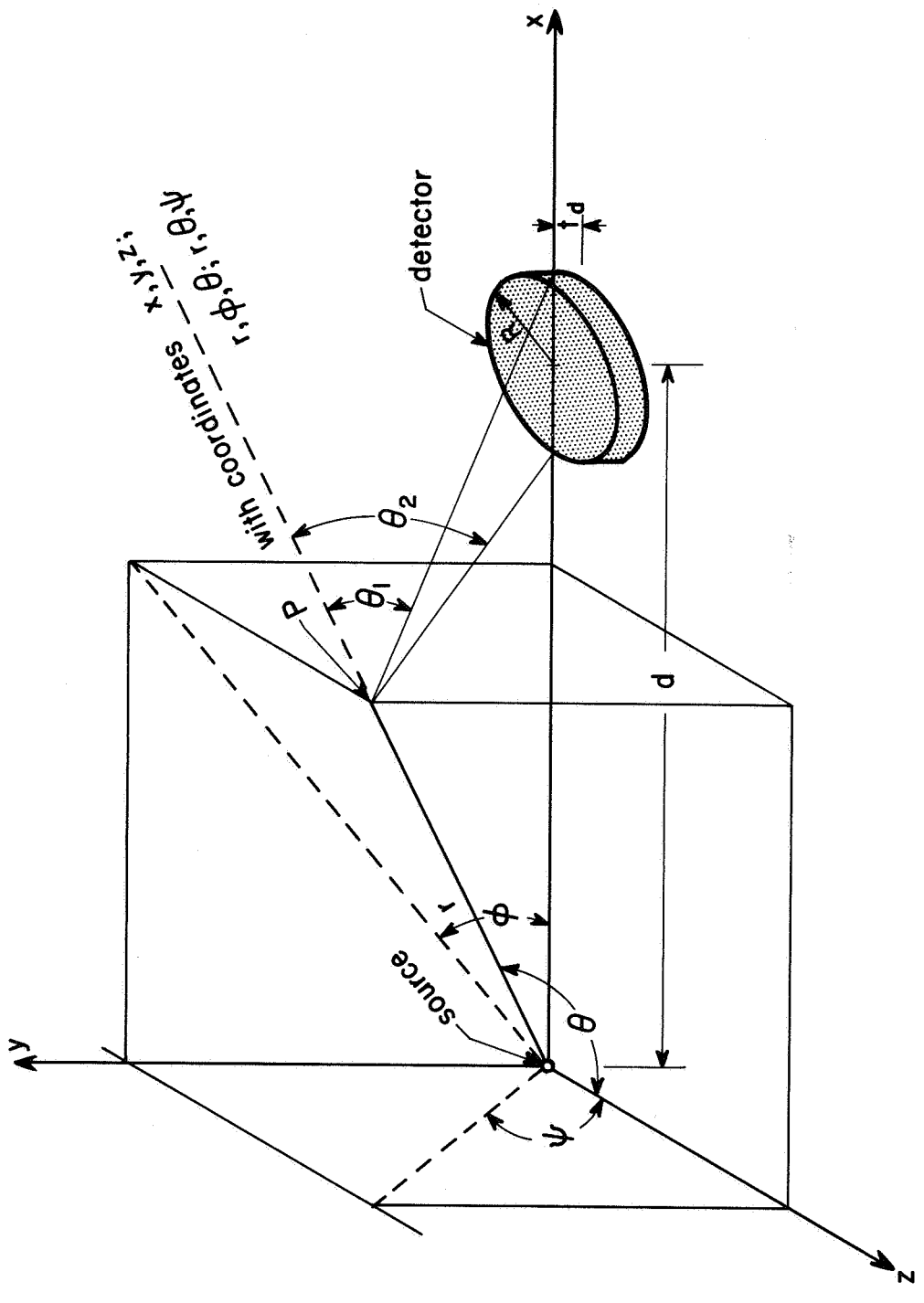

Fig. 3-1 Schematic diagram and coordinate systems of the gamma-ray scatter gauge

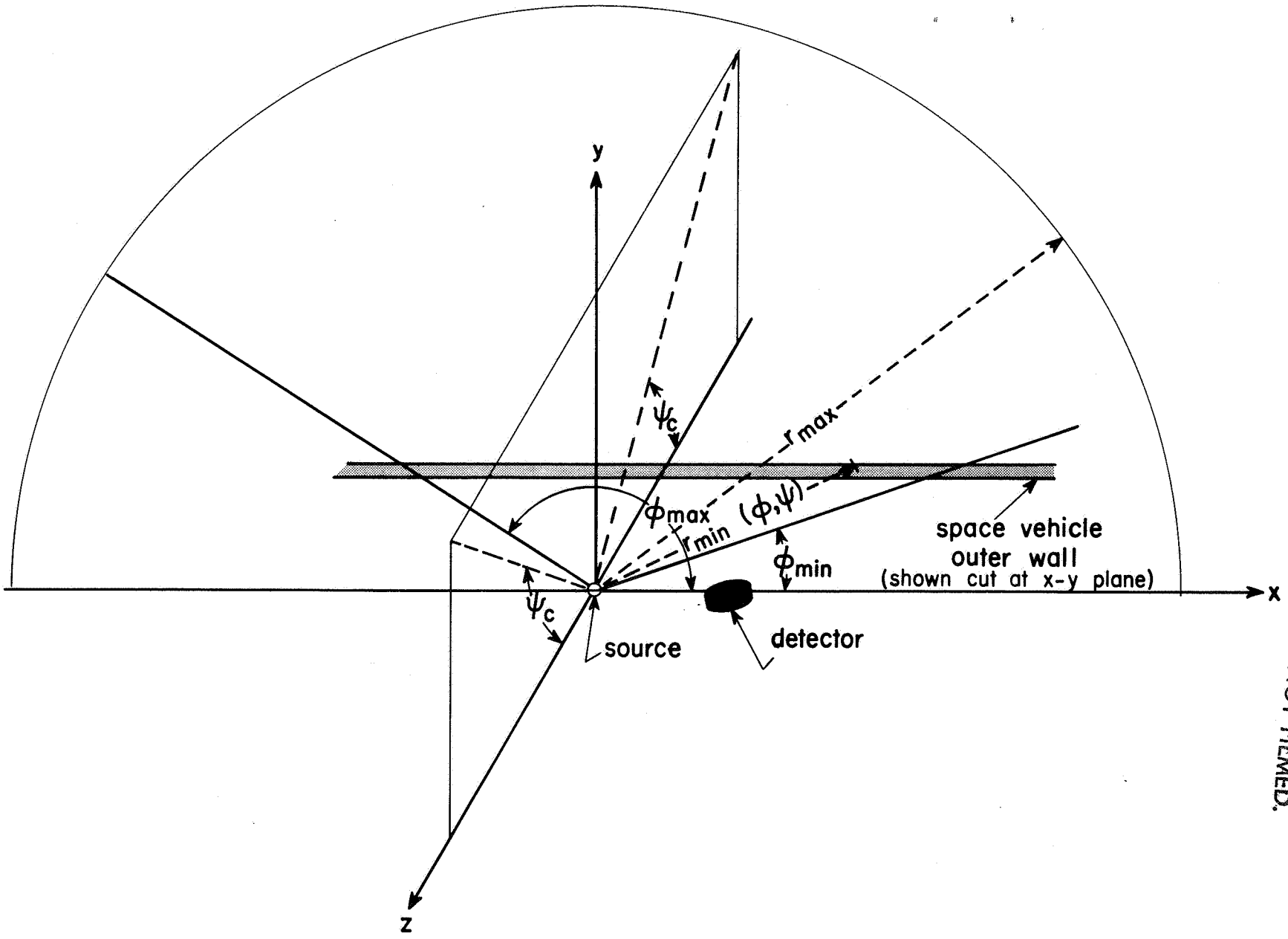

Fig. 3-2 Limiting values of integration on the gamma-ray signal response model

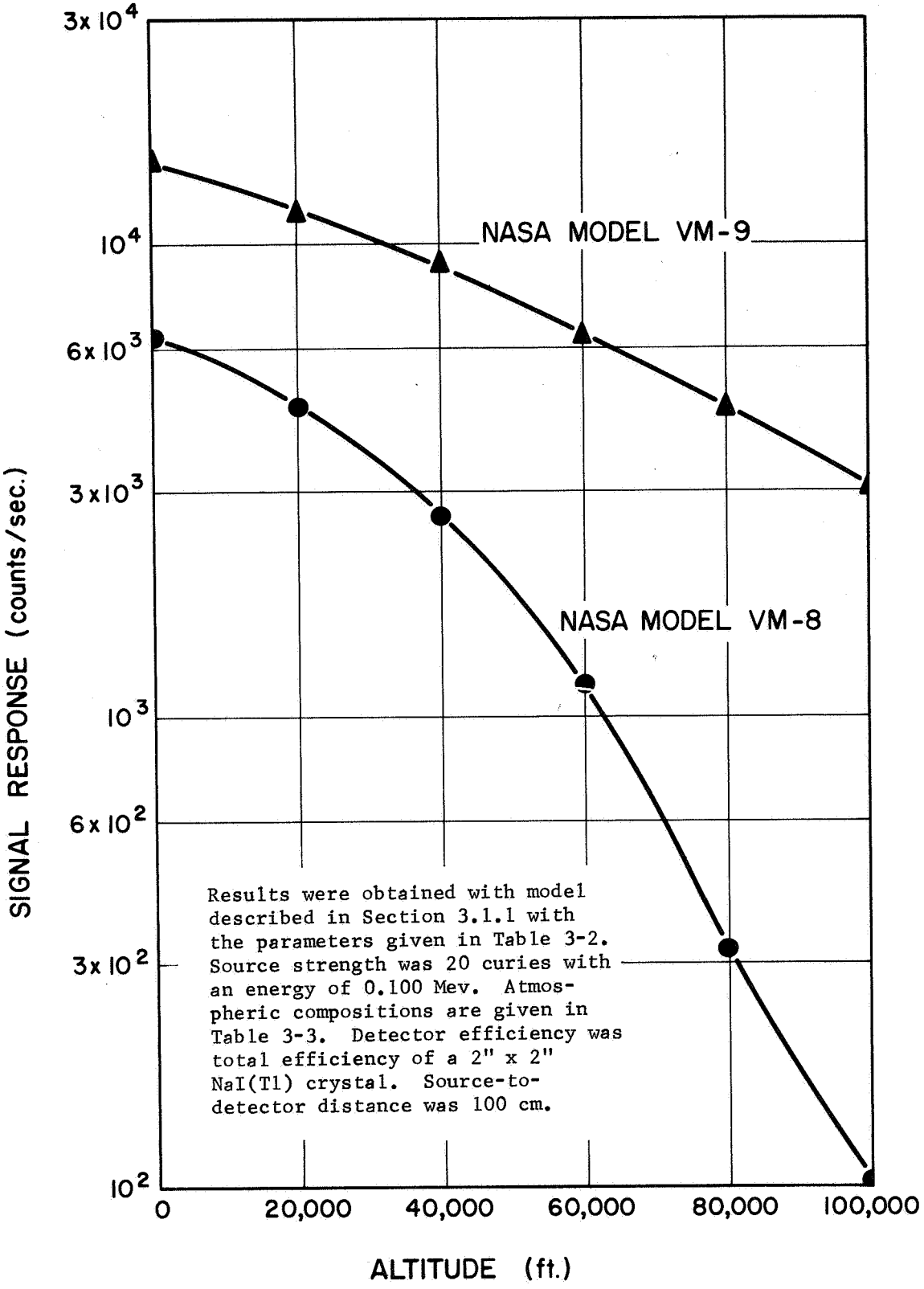

Fig. 3-3 Signal response as a function of altitude for the extremes of Mars model atmospheres

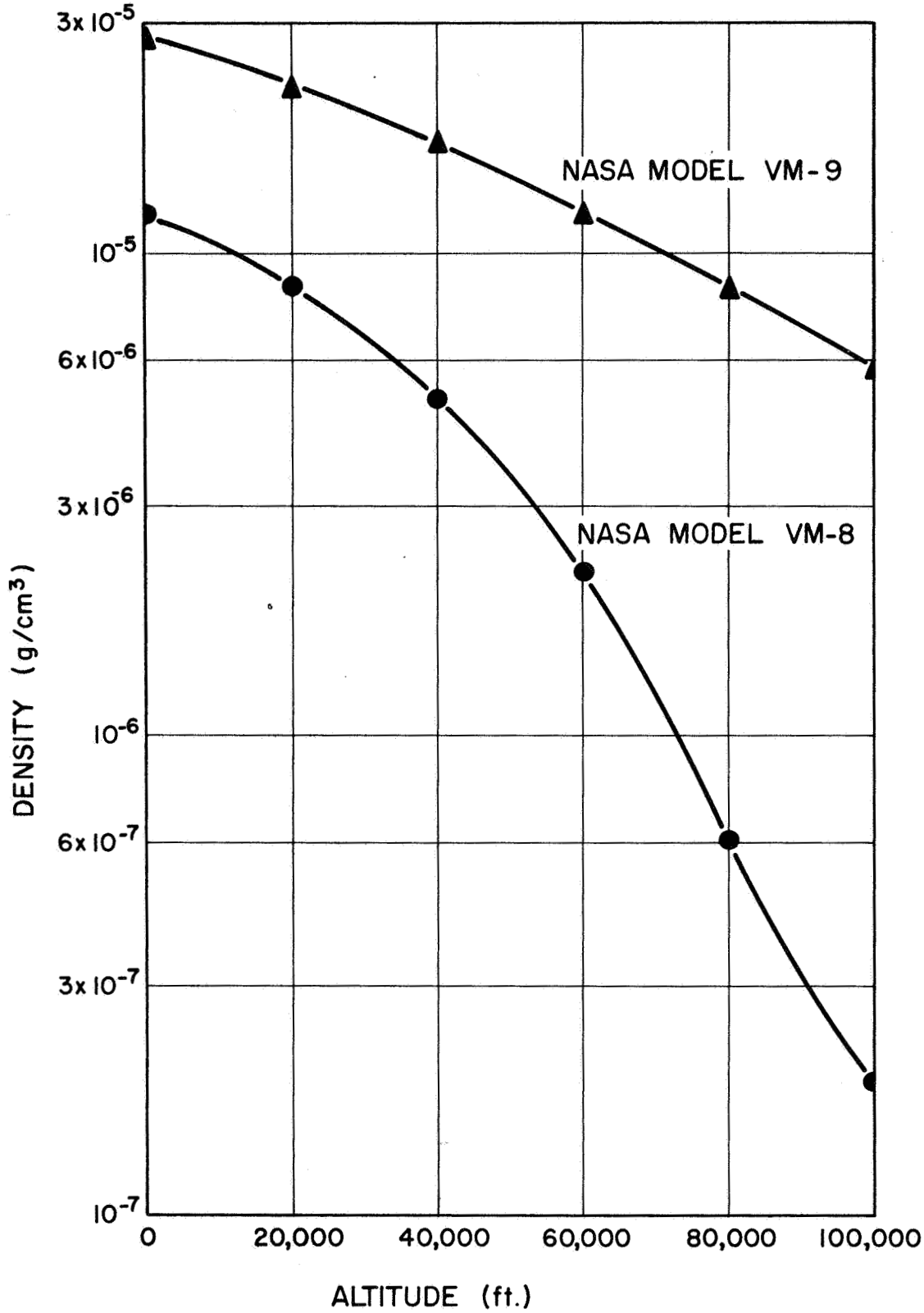

Fig. 3-4 Density as a function of altitude for the extremes of Mars model atmospheres

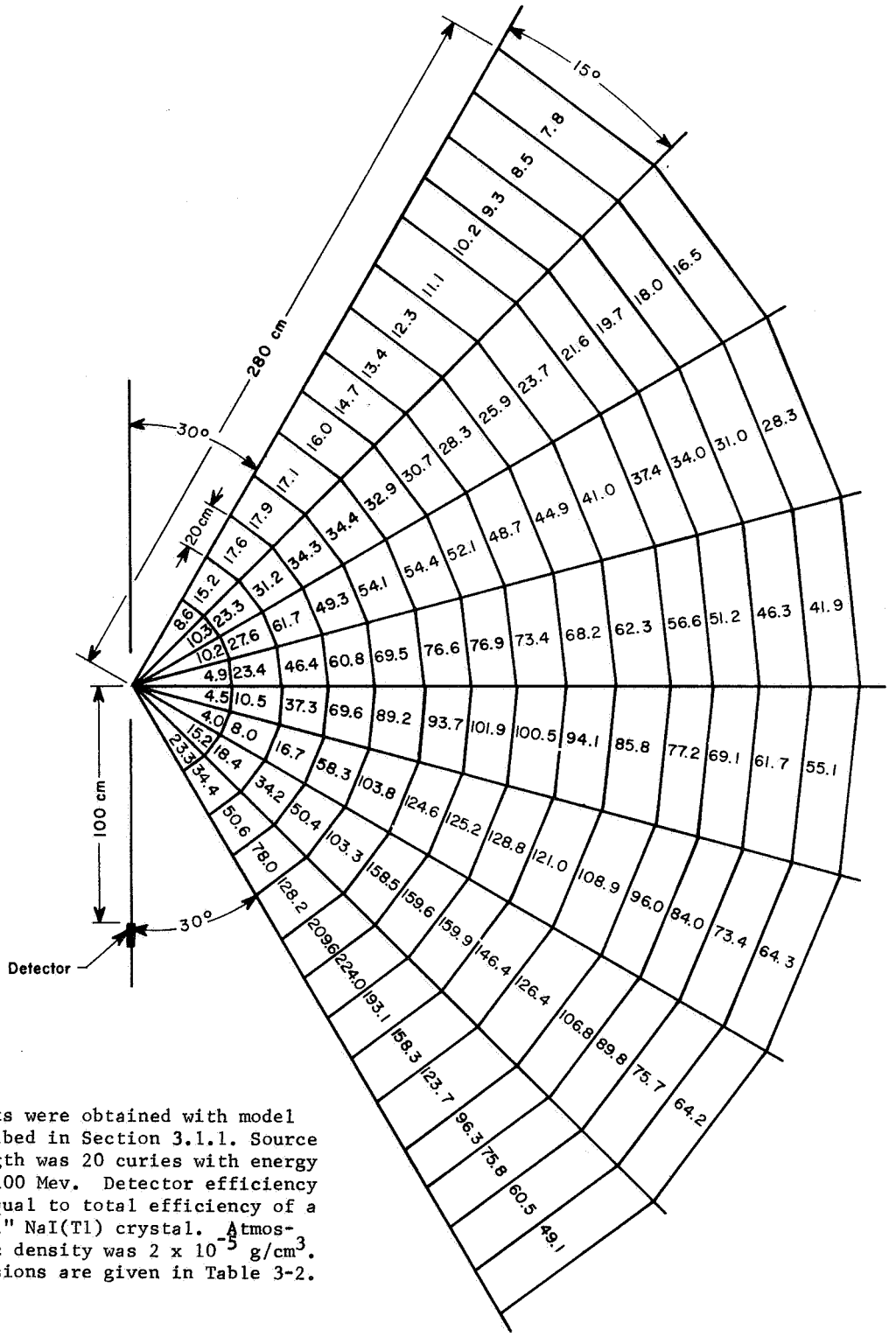

Results were obtained with model described in Section 3.1.1. Source strength was 20 curies with energy of 0.100 Mev. Detector efficiency was equal to total efficiency of a 2" x 2" NaI(Tl) crystal. Atmospheric density was 2×10^{-5} g/cm^3. Dimensions are given in Table 3-2.

Fig. 3-5A Predicted signal response per 10,000 total units at various distances from gauge

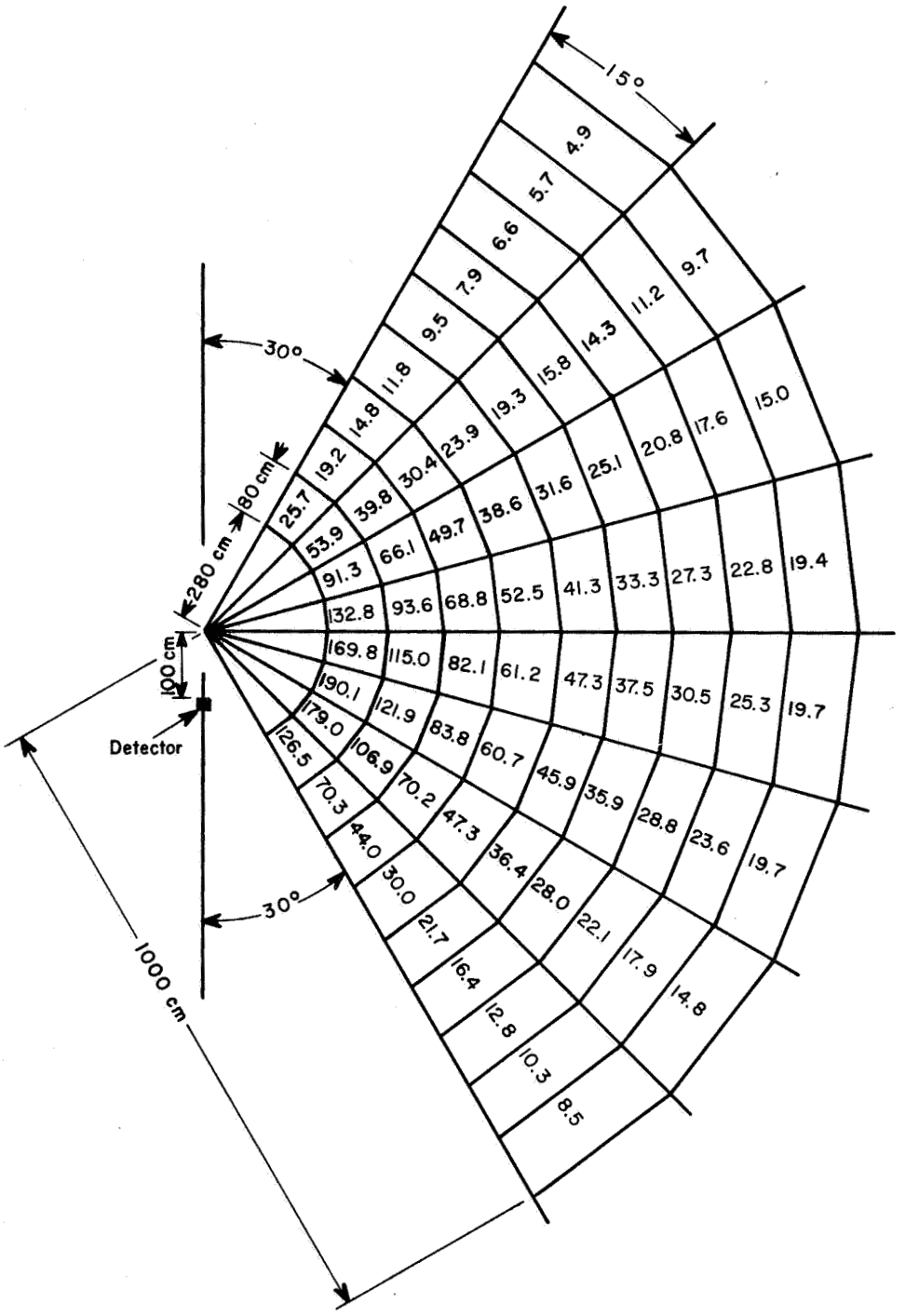

Fig. 3-5B Predicted signal response per 10,000 total units at various distances from gauge

Results were obtained with model described in Section 3.1.1. Source strength was 20 curies with energy of 0.100 Mev. Detector efficiency was equal to total efficiency of a 2" x 2" NaI(Tl) crystal. Atmospheric density was 2×10^{-5} g/cm^3. Dimensions are given in Table 3-2.

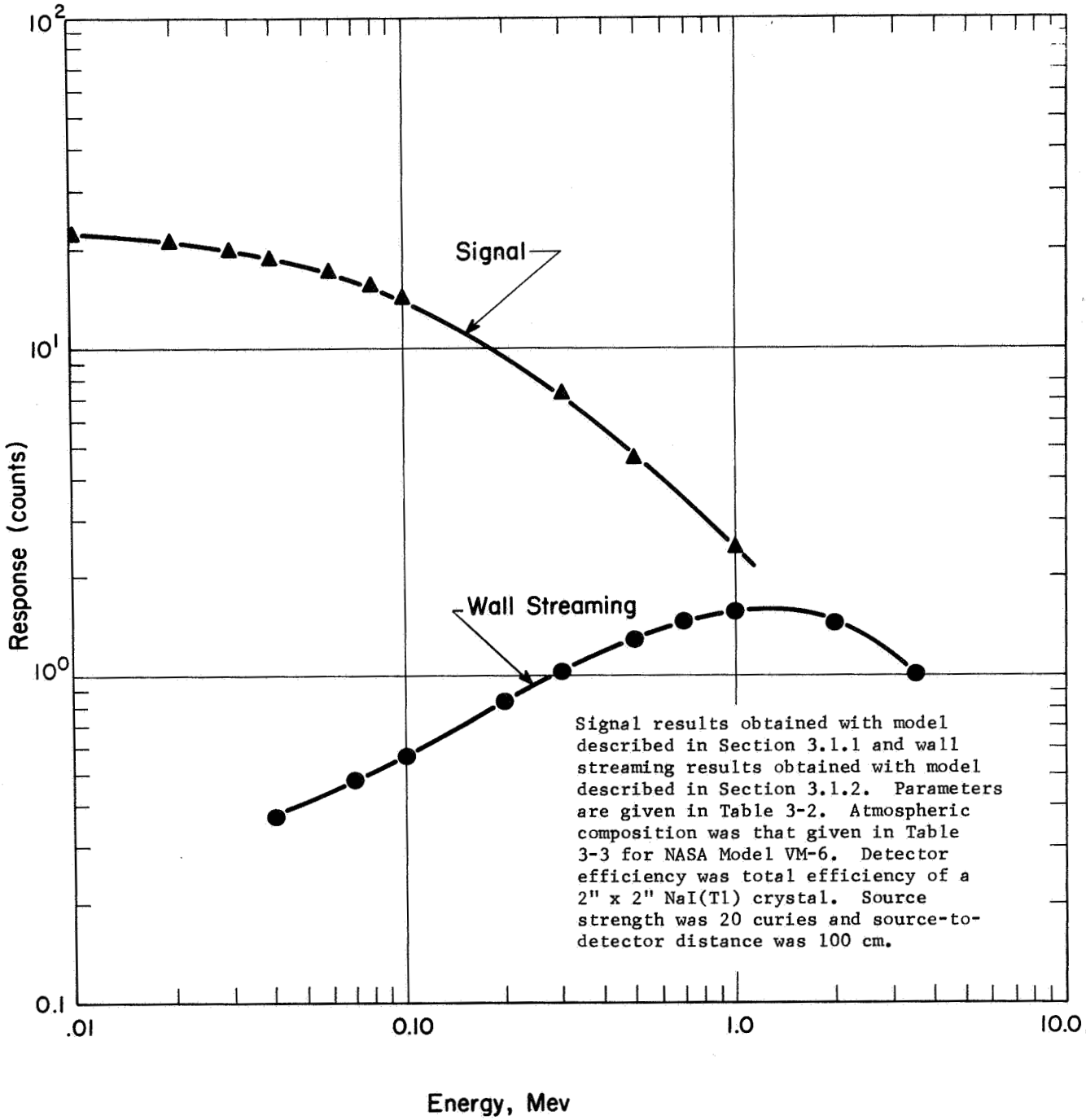

Fig. 3-6 Signal and wall streaming responses as a function of gamma-ray energy

TABLES

Table 3-1

RELATIONSHIPS BETWEEN CARTESIAN, SPHERICAL, AND

THE COORDINATE SYSTEM USED IN THIS STUDY

COORDINATE	CARTESIAN	SPHERICAL	THIS STUDY
r	$\sqrt{x^2 + y^2 + z^2}$	r	r
Φ	$\sin^{-1}\left[\frac{y}{\sqrt{x^2 + y^2}}\right]$	Φ	Φ
θ	$\cos^{-1}\left[\frac{z}{\sqrt{x^2 + y^2 + z^2}}\right]$	θ	$\cos^{-1}\left[\frac{1}{\sqrt{\tan^2 \psi \cot^2 \Phi + \tan^2 \psi + 1}}\right]$
ψ	$\sin^{-1}\left[\frac{y}{\sqrt{z^2 + y^2}}\right]$	$\tan^{-1}[\tan \theta \sin \Phi]$	Ψ
x	x	r sin θ cos Φ	$\frac{r}{\sqrt{1 + \tan^2 \Phi + \tan^2 \Phi \cot^2 \psi}}$
y	y	r sin θ sin Φ	$\frac{r}{\sqrt{\cot^2 \Phi + \cot^2 \psi + 1}}$
z	z	r cos θ	$\frac{r}{\sqrt{\tan^2 \psi \cot^2 \Phi + \tan^2 \psi + 1}}$

Table 3-2

DIMENSIONS OF GAUGE FOR 3-DIMENSIONAL STUDIES

ITEM	DESCRIPTION	DIMENSION
x_1	wall-to-source distance	5.0 cm
r_{max}	limit on r integration	1000 cm
t_w	wall thickness	.762 cm (phenolic) .3175 cm (aluminum)
ρ_w	wall density	0.25 g/cm^3 (phenolic) 2.699 g/cm^3 (aluminum)
	wall composition	12% Si, 24% O, 59% C and 5% H (phenolic) 100% Al (aluminum)
Φ_{min}	minimum limit on Φ	.7854 radians (45^o)
Φ_{max}	maximum limit on Φ	2.356 radians (135^o)
ψ_c	minimum limit on ψ	.7854 radians (45^o)
D	source-to-detector distance	100 cm
t_d	detector thickness	.635 cm
R	detector radius	5.08 cm
	source strength	20 curies (7.4×10^{11} γ's/sec)

Table 3-3

COMPOSITIONS OF EARTH AND MARS ATMOSPHERES

MASS FRACTIONS

COMPONENT	EARTH	MARS MODEL VM-6	MARS MODEL VM-8	MARS MODEL VM-9	MARS MODEL VM-10
CO_2	.001	.357	1.000	.282	.130
N_2	.755	.286	.000	.718	.620
A	.013	.357	.000	.000	.250
O_2	.231	.000	.000	.000	.000

Table 3-4

SIGNAL RESPONSE TO DENSITY VARIATIONS
INDUCED BY SHOCK WAVES*

$\Psi_C = \Phi_{min} = \Phi_{max}$	SIGNAL RESPONSE FOR VARIOUS COLLIMATION ANGLES FROM VERTICAL CENTERLINE OF SOURCE		
	$\pm 30^o$ (counts/sec)	$\pm 60^o$ (counts/sec)	$\pm 81^o$ (counts/sec)
Response for $\rho=1.8 \times 10^{-7}$ g/cm^3 with no shock wave	9.158	29.05	41.97
Response for $\rho=1.8 \times 10^{-7}$ g/cm^3 with 24 cm shock wave with $\rho=1.1 \times 10^{-6}$ g/cm^3	10.888	34.48	66.12
Error introduced by 24 cm shock wave	1.733 (18.9%)	5.43 (18.7%)	24.15 (57.5%)
Response for $\rho=2.6 \times 10^{-5}$ g/cm^3 with no shock wave	1,320	4,185	6,047
Response for $\rho=2.6 \times 10^{-5}$ g/cm^3 with 120 cm shock wave with $\rho=1.0 \times 10^{-4}$ g/cm^3	2,773	10,809	17,432
Error introduced by 120 cm shock wave	1,453 (110%)	6,624 (158%)	11,385 (188%)

* The results given here were obtained with the signal response model described in Sec. 3.1.1 with the parameters given in Table 3-2. In addition the gamma-ray energy was taken as 0.100 Mev, the atmospheric composition was that given in Table 3-3 for NASA Model VM-8, the detector efficiency was taken as that for discriminator settings of 65 and 115 Kev, the gamma-ray source strength was 20 curies, and the source-to-detector distance was 100 cm.

Table 3-5

SIGNAL RESPONSE AS A FUNCTION OF
GAMMA-RAY ENERGY FOR
NASA MODEL VM-6 MARS ATMOSPHERE*

GAMMA-RAY ENERGY (Mev)	SIGNAL RESPONSE TO MARS ATMOSPHERE (ρ=1.80 x 10^{-7} g/cm^3) (counts/sec)
0.010	.2198 x 10^2
0.020	.2198 x 10^2
0.030	.1988 x 10^2
0.040	.1879 x 10^2
0.060	.1691 x 10^2
0.080	.1538 x 10^2
0.100	.1412 x 10^2
0.300	.7272 x 10^1
0.500	.4599 x 10^1
1.000	.2445 x 10^1

* The results given here were obtained with the signal response model described in Sec. 3.1.1 with the parameters given in Table 3-2 and the atmospheric composition given in Table 3-3. In addition the detector efficiency was the total efficiency of a 2" x 2" NaI(Tl) scintillation crystal, the gamma-ray source strength was 20 curies, and the source-to-detector distance was 100 cm. The wall was 0.50 cm thick phenolic with a density of 0.50 g/cm^3.

Table 3-6

WALL-STREAMING RESPONSE AS A FUNCTION OF GAMMA-RAY ENERGY FOR TWO WALL MATERIALS*

GAMMA-RAY ENERGY (Mev)	STREAMING RESPONSE FOR PHENOLIC WALL (ρ=0.25 g/cm^3) (counts/sec)	STREAMING RESPONSE FOR ALUMINUM WALL (ρ=2.699 g/cm^3) (counts/sec)
0.040	0.3684	0.3447×10^{-16}
0.070	0.4690	0.1085×10^{-14}
0.100	0.5615	0.1347×10^{-13}
0.200	0.8270	0.2812×10^{-11}
0.300	1.0131	0.5750×10^{-10}
0.500	1.2858	0.1790×10^{-8}
0.700	1.4619	0.1270×10^{-7}
1.000	1.5840	0.7440×10^{-7}
2.000	1.4413	0.8883×10^{-6}
3.500	1.0029	0.2721×10^{-5}

* The results given here were obtained with the wall streaming response model described in Sec. 3.1.2 with the parameters given in Table 3-2. In addition the detector efficiency was the total efficiency of a 2" x 2" NaI (Tl) scintillation crystal, the gamma-ray source strength was 20 curies, and the source-to-detector distance was 100 cm.

Table 4-1

RESULTS FOR OPTIMIZATION OF DETECTOR THICKNESS, SOURCE-TO-DETECTOR DISTANCE, AND LOWER AND UPPER DISCRIMINATOR SETTINGS

Fixed Variables				Searched Variables				Calculated Gauge Characteristics				
									Noise			
Shield Weight	Collimation Angles, ψ_c	Wall Material	Wall Thickness	Detector Thickness	Source-To-Detector Distance	Lower Disc. Setting	Upper Disc. Setting	Signal	Cosmic	Stream	Direct	Ratio Noise/Signal
(Grams)	(degrees)		(cm)	(cm)	(cm)	(Mev)	(Mev)	(counts/sec)	(counts/sec)	(counts/sec)	(counts/sec)	
2000	±45	Phenolic	0.762	.6350	554.2	.06036	.07998	2.932×10^{2}	$.3174\times10^{-4}$	$.1890\times10^{-8}$	$< 10^{-39}$	$.1083\times10^{-6}$
1000	±45	Phenolic	0.762	.6350	554.2	.06036	.07998	2.932×10^{2}	$.3174\times10^{-4}$	$.1890\times10^{-8}$	$.2886\times10^{-21}$	$.1083\times10^{-6}$
500	±45	Phenolic	0.762	.6350	554.2	.06036	.07998	2.932×10^{2}	$.3174\times10^{-4}$	$.1890\times10^{-8}$	$.1158\times10^{-8}$	$.1083\times10^{-6}$
2000	±30	Phenolic	0.762	.6350	554.2	.06036	.07998	1.978×10^{2}	$.3174\times10^{-4}$	$.6711\times10^{-9}$	$< 10^{-39}$	$.1605\times10^{-6}$
1000	±30	Phenolic	0.762	.6350	554.2	.06036	.07998	1.978×10^{2}	$.3174\times10^{-4}$	$.6711\times10^{-9}$	$.2886\times10^{-21}$	$.1605\times10^{-6}$
500	±30	Phenolic	0.762	.6350	554.2	.06036	.07998	1.978×10^{2}	$.3174\times10^{-4}$	$.6711\times10^{-9}$	$.1158\times10^{-8}$	$.1605\times10^{-6}$
2000	±45	Aluminum	0.3175	.7059	67.66	.04995	.1510	8.414×10^{3}	$.6671\times10^{-3}$	$.2424\times10^{-7}$	$< 10^{-39}$	$.7929\times10^{-7}$
1000	±45	Aluminum	0.3175	.7059	67.66	.04995	.1510	8.414×10^{3}	$.6671\times10^{-3}$	$.2424\times10^{-7}$	$.8444\times10^{-25}$	$.7929\times10^{-7}$
500	±45	Aluminum	0.3175	.7059	67.66	.04995	.1510	8.414×10^{3}	$.6671\times10^{-3}$	$.2424\times10^{-7}$	$.1531\times10^{-9}$	$.7929\times10^{-7}$
2000	±45	Phenolic	1.08	.6350	554.2	.06036	.07998	2.981×10^{2}	$.4168\times10^{-4}$	$.3973\times10^{-8}$	$< 10^{-39}$	$.1399\times10^{-6}$
1000	±45	Phenolic	1.08	.6350	554.2	.06036	.07998	2.981×10^{2}	$.4168\times10^{-4}$	$.3973\times10^{-8}$	$.2886\times10^{-21}$	$.1399\times10^{-6}$
500	±45	Phenolic	1.08	.6350	554.2	.06036	.07998	2.981×10^{2}	$.4168\times10^{-4}$	$.3973\times10^{-8}$	$.1158\times10^{-8}$	$.1399\times10^{-6}$

The results given here were obtained with the master optimization computer program described in Sec. 4.1. In addition the gamma ray energy was taken as 0.100 Mev, the atmospheric composition was that given in Table 3-3 for NASA Model VM-10 with a density of 1.60×10^{-5} g/cm^3, the gamma-ray source strength was 20 curies, and the other parameters are as shown.

Table 4-2

RESULTS FOR OPTIMIZATION OF SOURCE ENERGY AND LOWER AND UPPER DISCRIMINATOR SETTINGS

Fixed Variables			Searched Variables			Calculated Gauge Characteristics				
							Noise			
Shield Weight	Wall Thickness	Source-to-Detector Distance	Optimum Source Energy	Lower Disc. Setting	Upper Disc. Setting	Signal	Cosmic	Stream	Direct	Ratio Noise/Signal
(Grams)	(cm)	(cm)	(Mev)	(Mev)	(Mev)	(counts/sec)	(counts/sec)	(counts/sec)	(counts/sec)	
2000	0.762	150	.07633	.04529	.0677	3.2318×10^{3}	$.3621 \times 10^{-4}$	$.3514 \times 10^{0}$	$< 10^{-39}$	$.1087 \times 10^{-3}$
1000	0.762	150	.07633	.04529	.0677	3.2318×10^{3}	$.3621 \times 10^{-4}$	$.3514 \times 10^{0}$	$.5912 \times 10^{-29}$	$.1087 \times 10^{-3}$
500	0.762	150	.07633	.04529	.0677	3.2318×10^{3}	$.3621 \times 10^{-4}$	$.3514 \times 10^{0}$	$.5610 \times 10^{-12}$	$.1087 \times 10^{-3}$
2000	1.08	150	.07633	.04529	.0677	3.171×10^{3}	$.4748 \times 10^{-4}$	$.6824 \times 10^{0}$	$< 10^{-39}$	$.2152 \times 10^{-3}$
1000	1.08	150	.07633	.04529	.0677	3.171×10^{3}	$.4748 \times 10^{-4}$	$.6824 \times 10^{0}$	$.5912 \times 10^{-29}$	$.2152 \times 10^{-3}$
500	1.08	150	.07633	.04529	.0677	3.171×10^{3}	$.4748 \times 10^{-4}$	$.6824 \times 10^{0}$	$.5610 \times 10^{-12}$	$.2152 \times 10^{-3}$
2000	0.762	100	.110	.07760	.1500	3.430×10^{3}	$.1179 \times 10^{-3}$	$.4632 \times 10^{1}$	$< 10^{-39}$	$.1350 \times 10^{-2}$
1000	0.762	100	.110	.07760	.1500	3.430×10^{3}	$.1179 \times 10^{-3}$	$.4632 \times 10^{1}$	$.1330 \times 10^{-28}$	$.1350 \times 10^{-2}$
500	0.762	100	.110	.07760	.1500	3.430×10^{3}	$.1179 \times 10^{-3}$	$.4632 \times 10^{1}$	$.1262 \times 10^{-11}$	$.1350 \times 10^{-2}$
2000	0.762	50	.110	.07760	.1500	6.403×10^{3}	$.1179 \times 10^{-3}$	$.1241 \times 10^{3}$	$< 10^{-39}$	$.194 \times 10^{-1}$
1000	0.762	50	.110	.07760	.1500	6.403×10^{3}	$.1179 \times 10^{-3}$	$.1241 \times 10^{3}$	$.5321 \times 10^{-28}$	$.194 \times 10^{-1}$
500	0.762	50	.110	.07760	.1500	6.403×10^{3}	$.1179 \times 10^{-3}$	$.1241 \times 10^{3}$	$.5049 \times 10^{-11}$	$.194 \times 10^{-1}$

The results given here were obtained with the same parameters as shown in Table 4-1. All walls were phenolic resin, the detector thickness was always 0.6350 cm, and the collimation angles were $\pm 45°$.

Table 4-3

MIZATION RESULTS FOR SOURCE ENERGY, SOURCE-TO-DETECTOR DISTANCE, AND LOWER AND UPPER DISCRIMINATOR SETTINGS

Fixed Variables

Shield Weight: 2000 grams
Collimation Angles: $\pm 45^{o}$
Wall Material: Phenolic
Wall Thickness: 0.762 cm
Detector Thickness: 0.6350 cm

Searched Variables

Source Energy: 106.4 Kev
Source-to-Detector Distance: 224.7 cm
Lower Discriminator Setting: 67.15 Kev
Upper Discriminator Setting: 83.50 Kev

Calculated Gauge Characteristics

Signal: 1.999×10^{3} counts/sec
Cosmic Noise: 0.1637 counts/sec
Streaming Noise: 0.05580 counts/sec
Direct Transmission Noise: $<10^{-39}$ counts/sec
Variance: $.2812 \times 10^{-16}$ g^2/cm^6
Standard Deviation: $.530 \times 10^{-8}$ g/cm^3

Note: The results given here were obtained by using the master optimization computer program described in Sec. 4.1. The parameters other than those listed are given in Table 3-2.

Table 4-4

OPTIMIZATION RESULTS FOR SOURCE-TO-DETECTOR DISTANCE AND UPPER AND LOWER DISCRIMINATOR SETTINGS

Fixed Variables

Shield Weight: 2000 grams
Collimation Angles: $\pm 45^{o}$
Wall Material: Phenolic
Wall Thickness: 0.762 cm
Detector Thickness: 0.6350 cm
Source Energy: 100 Kev

Searched Variables

Source-to-Detector Distance: 247.9 cm
Lower Discriminator Setting: 65.86 Kev
Upper Discriminator Setting: 106.6 Kev

Calculated Gauge Characteristics

Signal: 2.2052×10^{3} counts/sec
Cosmic Noise: 0.4073 counts/sec
Streaming Noise: 0.02397 counts/sec
Direct Transmission Noise: $<10^{-39}$ counts/sec
Variance: $.4541 \times 10^{-16}$ g^2/cm^6
Standard Deviation: $.675 \times 10^{-8}$ g/cm^3

Note: The results given here were obtained by using the master optimization computer program described in Sec. 4.1. The parameters other than those listed are given in Table 3-2.

APPENDIX A

DETECTOR EFFICIENCY MODEL

Scintillating crystals convert to a pulse of light a proportional amount of that energy from a gamma-ray interaction that is imparted to the participating electron. Both the photoelectric effect interaction which imparts all of the gamma-ray energy to an electron and the Compton scattering interaction (or multiple Compton scattering interactions) which can impart any energy up to a maximum dictated by the original energy of the gamma ray can occur in any single interaction of a gamma ray with a scintillating crystal. A typical spectrum of the light pulses that have been converted to voltage pulses (pulse-height spectrum) from a monoenergetic source of gamma rays interacting with a scintillating crystal is shown in Fig. A-1. The photopeak and Compton continuum are identified. The Compton continuum was divided into two parts, a rectangular area and a triangular area as shown in Fig. A-1. The area under the total curve (total number of pulses) divided by the number of gamma rays that intercepted the detector is the total efficiency E_t of the crystal for the particular gamma-ray energy illustrated. The total efficiency of the crystal is given by

$$E_t = 1 - e^{-\mu_d x} \qquad \text{(A-1)}$$

where μ_d is the total attenuation coefficient of the crystal, in cm^{-1},

and x is the effective detector thickness, in cm.

The μ_d term is again similar to the μ_t term of Eq. (3.1.1-2) and the μ_s term of Eq. (3.1.4-4). It is composed of the total Compton scattering probability in the NaI crystal and the photoelectric effect probability in NaI. The Compton probability was computed as usual and the photoelectric probability was computed by the equation

$$\tau_d = a\, E^b \ cm^{-1} \qquad \text{(A-2)}$$

where a and b are empirical constants

and E is the gamma-ray energy, in Mev.

The constants a and b were determined by taking values of the photoelectric attenuation coefficients for NaI(Tl) crystals at two energies from Table 3.1 of Crouthamel [10] and solving the resulting equations simultaneously. The constant a was found to be 0.0142 and b was -2.62.

The effective detector thickness x was taken as the distance through the center of the detector intercepted by the scattered gamma ray. This thickness can be expressed by the equation

$$x = \frac{t}{y_1}\sqrt{(x_1 - D)^2 + y_1^2 + z_1^2} \quad \text{cm} \qquad \text{(A-3)}$$

where t is detector thickness, in cm,

D is source-detector distance, in cm,

and x_1, y_1, z_1, are coordinates of the scatter point, in cm.

In the signal response model x_1, y_1, z_1 are coordinates of the one scatter for each gamma ray and in the wall streaming response model these are the coordinates of the second scatter point.

The fraction of the total area under the curve in Fig. A-1 that is in the photopeak is called the photofraction, or peak-to-total ratio. This ratio can be expressed as

$$PR = \left[\frac{1 - e^{-\tau_d x}}{1 - e^{-\mu_d x}}\right]^c \qquad \text{(A-4)}$$

where c is an empirical parameter

and τ_d, μ_d and x are as defined earlier.

The parameter c was determined by plotting the experimental peak-to-total ratios shown on page 336 of Crouthamel [10] for a NaI(Tl) crystal versus energy and

determining c so that the computed peak-to-total ratios would fit this curve. This parameter c was found to be of the form

$$c = a\ e^{bE} \tag{A-5}$$

where a and b are empirical parameters

and E is gamma-ray energy, in Mev.

The parameters a and b varied depending on the gamma-ray energy.

For this model the shape of the photopeak was taken as a normal (or Gaussian) distribution with the resolution being computed by

$$\text{Res} = \sqrt{\alpha + \beta/E} \tag{A-6}$$

where α and β are constants

and E is gamma-ray energy, in Mev.

There are no units on Res when the energy is in Mev. The constants α and β were taken from Fig. 2-3 of Crouthamel [10] and were equal to 4.5×10^{-3} and 1.57×10^{-3}, respectively. These values give a resolution of 8.3% for a 0.662 Mev gamma ray.

The Compton continuum was divided into two parts as discussed earlier with the upper limit of the rectangular part being the maximum energy that can be imparted to an electron by a gamma ray of the energy employed in one Compton scattering interaction. This maximum electron energy T_{max} (c.f. Evans [8]) is given by:

$$T_{max} = \frac{2E^2}{0.511 + 2E} \quad \text{Mev} \tag{A-7}$$

Now the area under the total curve is equal to the total efficiency, or

$$A_p + A_c = E_t \tag{A-8}$$

where A_p is the area under the photopeak portion of the spectrum

and A_c is the area under the Compton continuum portion of the spectrum.

But the peak-to-total ratio is given by:

$$PR = \frac{A_p}{A_p + A_c} . \tag{A-9}$$

Therefore the area under the Compton continuum can be computed by:

$$A_c = E_t \ (1 - PR) \tag{A-10}$$

The height h of the Compton continuum can now be found by:

$$h = \frac{A_c}{[T_{max} + 0.50 \ (E - 0.50 \ (E - T_{max}) - T_{max})]} \tag{A-11}$$

where T_{max} and E are in Mev.

The efficiency can be seen to be the sum of the areas in the Compton continuum and the photopeak. With the equation given above, the efficiency for a given crystal operated between any two energy discrimination levels for any gamma-ray energy can be calculated.

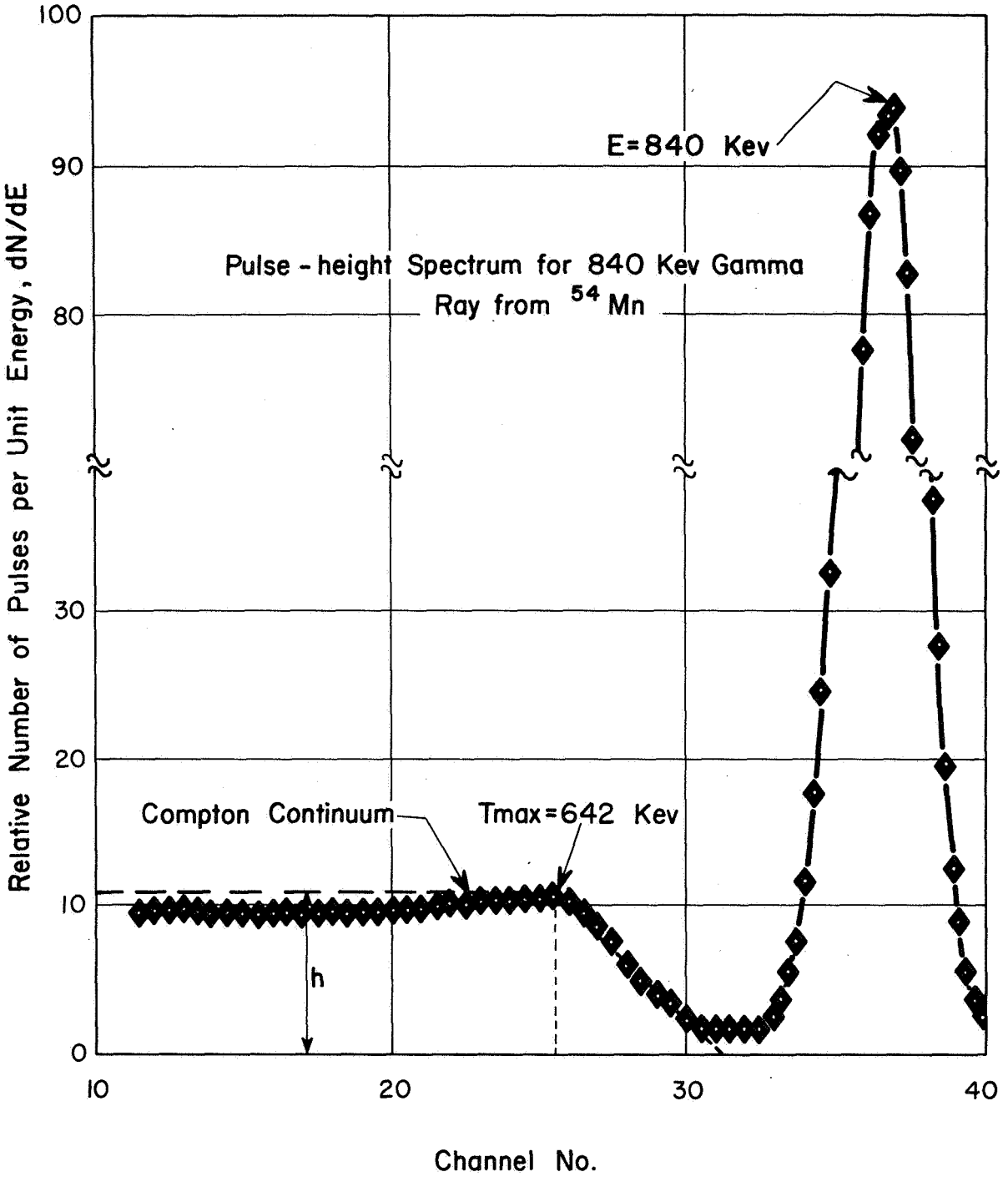

Fig A-1 Typical monoenergetic gamma-ray, pulse-height spectrum using a NaI(Tl) crystal and photomultiplier

APPENDIX B

DETECTOR SOLID ANGLE MODEL

Figure B-1 gives the pertinent nomenclature of the circular face of a cylindrical detector with respect to the origin or the point source of radiation. The differential angle subtended is given by:

$$d\Omega = \frac{\cos \theta' \, r \, dr \, d\Phi}{d^2} \tag{B-1}$$

By using appropriate geometrical identities and integrating from r = 0 to r = R, one obtains

$$\Omega = 2h \int_0^{\pi} \left\{ \frac{D}{(D^2 - \rho^2 \cos^2 \Phi)} - \frac{\rho R \cos \Phi + D^2}{(D^2 - \rho^2 \cos^2 \Phi) \sqrt{D^2 + R^2 + 2\rho R \cos \Phi}} \right\} d\Phi \tag{B-2}$$

Rearranging and integrating the first term of Eq. (B-2) gives:

$$\Omega = 2\Pi - \frac{2\sqrt{1 - (\rho/D)^2}}{\sqrt{1 + (R/D)^2}} \int_0^{\pi} \frac{[\, 1 + (R/D)\,(\rho/D) \cos \Phi \,]}{[\, 1 - (\rho/D)^2 \cos^2 \Phi]\sqrt{1 + b\,(\rho/D) \cos \Phi}} \, d\Phi \tag{B-3}$$

$$\text{where} \quad b = \frac{2RD}{D^2 + R^2}$$

By expanding the integrand of Eq. (B-3) in an infinite series and integrating term by term, one obtains the solution:

$$\Omega = 2\Pi - \frac{2\Pi\sqrt{1 - (\rho/D)^2}}{\sqrt{1 + (R/D)^2}} \left(1 + \sum_{i=1}^{\infty} x_i \right) \tag{B-4}$$

$$\text{where} \quad x_i = \left(A_{2i} - (R/D)\, A_{2i-1} \right) (\rho/D)^{2i} \prod_{j=1}^{i} \frac{2j-1}{2j} \, ,$$

$$A_k = A_{k-2} + b^k \prod_{j=1}^{k} \frac{2j-1}{2j} \quad , \text{(for } k > 2\text{)}$$

$$A_1 = 1/2b,$$

and $$A_2 = 3/8b^2 + 1$$

This is the solution given by Zumwalt [11].

For small solid angles it is obvious that the solution given by Eq. (B-4) would involve subtracting one large number from another. Assuming that one would want to obtain this solution on a digital computer without having to use double precision format, the solution given by Eq. (B-4) would not be accurate for solid angles smaller than about 10^{-4}. (This assumes that the computer carries six significant figures). If one tries to eliminate this problem by expanding $\sqrt{1 - \rho^2/D^2}$, $\sqrt{1 + R^2/D^2}$, or both into a series, it is found that the expansions are valid only for certain ranges of values of ρ/D and R/D. An alternate approach to the problem is to derive another series solution of more appropriate form.

If rather than integrating the first term inside the integral of Eq. (B-2) it is combined with the second term and expanded in an infinite series, then one obtains the alternate solution:

$$\Omega = \frac{2\pi\sqrt{1 - (\rho/D)^2}}{\sqrt{1 + (R/D)^2}} \left(\sqrt{1 + (R/D)^2} - 1 + \sum_{i=1}^{\infty} y_i\right) \qquad \text{(B-5)}$$

$$\text{where } y_i = \left[\left(\sqrt{1 + (R/D)^2} - 1\right) B_{i+1} - \sum_{j=1}^{i} B_{i-j+1} C_{j+1} \right] \prod_{j=1}^{i} \frac{2j-1}{2j}, \quad (i>o)$$

$$B_1 = 1$$

$$C_1 = 1$$

$$B_k = (\rho/D)^{2k-2} \prod_{j=1}^{k-1} \frac{2j-1}{2j} \quad , \quad (k>1)$$

$$C_k = \left(\left(\frac{4k-5}{4k-4}\right) F_1 - \rho\, R/D^2 \right) F_1 \prod_{j=1}^{2k-3} \frac{2j-1}{2j} \quad , \quad (k>1)$$

and $$F_1 = \frac{2\,(\rho/D)\,(R/D)}{1 + (R/D)^2} \, .$$

In this model it was found that the first five terms of Eq. (B-5) provided reasonable accuracy. Therefore, this was programmed in FORTRAN II and run on the Bunker-Ramo 340.

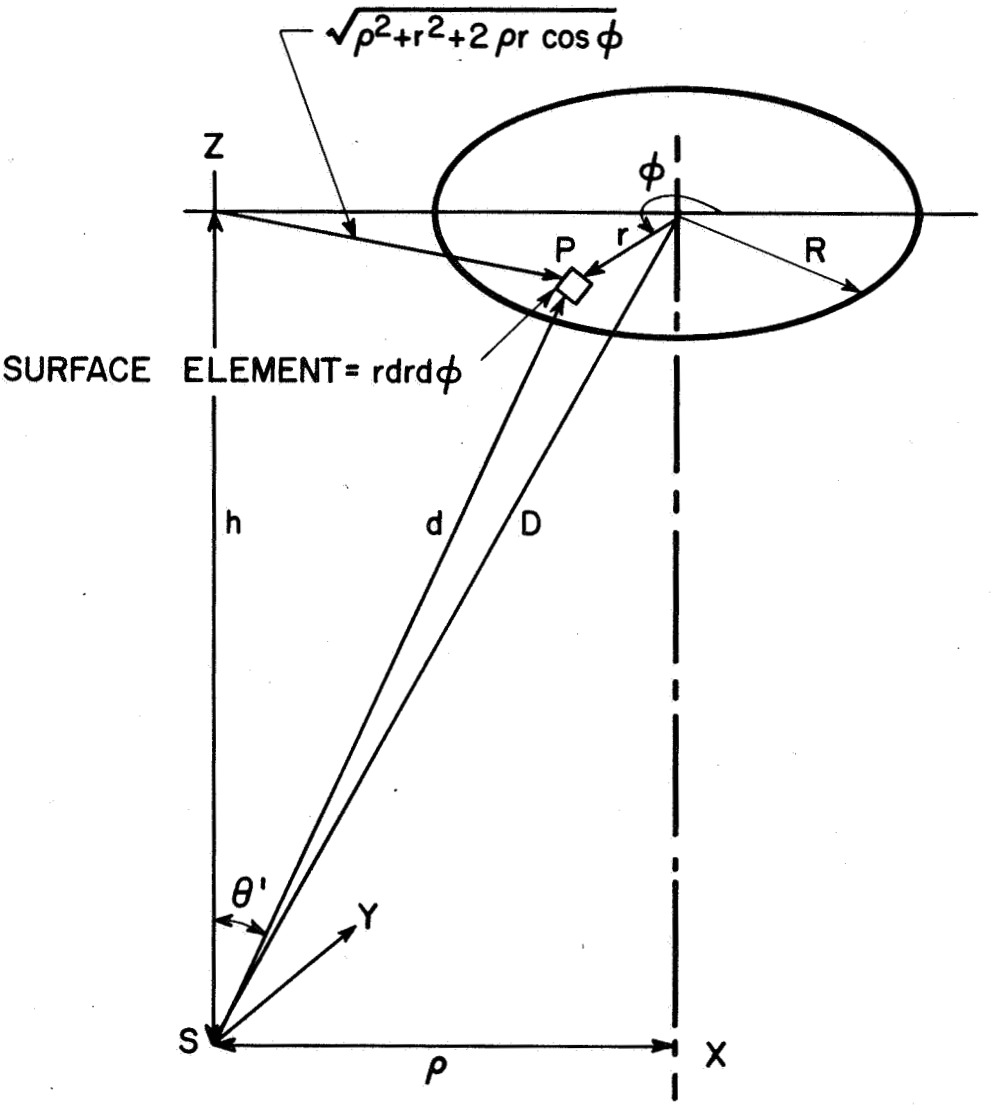

Fig. B-1 Schematic drawing of solid angles subtended by a circle